Block Copolymer Self-assembly and Graphene Dry Etching

by

Wadha Alyalak

A thesis
presented to the University of Waterloo
in fulfillment of the
thesis requirement for the degree of
Master of Applied Science
in
Mechanical Engineering- Nanotechnology

Waterloo, Ontario, Canada, 2015

AUTHOR'S DECLARATION

I hereby declare that I am the sole author of this thesis. This is a true copy of the thesis, including any required final revisions, as accepted by my examiners.

I understand that my thesis may be made electronically available to the public.

Abstract

This thesis focuses on interpreting the use of block copolymer self-assembly in nanolithography. Block copolymers are attractive materials for nanofabrication due to their ability to phase separate into ordered and chemically distinct domains of 10s nm size. In order to utilize the self-assembled structure in lithography applications like pattern transfer, the structure has to be perpendicular to the substrate. This thesis presents an effective way to deliver a perpendicular self-assembled PS-b-PMMA using 3-MPTS to neutralize the surface. This method depends on vapor deposition of 3-MPTS at room temperature for two hours prior to deposition of PS-b-PMMA.

This thesis also presents an easy and effective way to control the number of graphene layers based on RIE process using oxygen plasma. The etching process was preformed on multi and single layer graphene prepared by (CVD). Raman spectrometer was used to characterize the samples before and after RIE process. The number of layers was identified form Raman spectrum by calculating the ratio I2D/IG, and the results show that bi-layer and single layer were achieved from multi-layer graphene, and the graphene was etched when using RIE process on a single-layer graphene. The RIE process was successfully used to pattern-transfer on a graphene-oxide film. This presents an effective solution to pattern and etch graphene for different applications.

Acknowledgements

I would like to express my sincere gratitude to my supervisor professor Mustafa Yavuz and my co-supervisor professor Bo Cui for their continuous support and gaudiness throughout my study and research. Their guidance and patience helped me face and overcome all the challenges that crossed my way during my work on this research.

I also would like to express my heartfelt appreciation to Dr. Mehrdad Irannejad for his unconditional assistance and support. He has always been there for any question offering the ultimate guidance.

Special thanks go to my friends and colleagues Khaled Ibrahim and Mervat Alamri for their help and assistance in using Origin software; they have offered and delivered all their knowledge to help me with it. I also thank all my group members without any exception for their help and support throughout my studies. With great pleasure, I thank Ritchard Barber the manager of G2N lab for his help along with everyone I worked with there.

Special thanks go to my dear friend Shaima Sawan for her support and encouragement throughout my study.

I am privileged to have been granted a scholarship from my country Saudi Arabia. I am thankful for the Saudi Cultural Bureau in Canada for their constant support and encouragement that made my dream of pursuing my graduate studies in Canada and specifically in the University of Waterloo possible.

I owe my deepest gratitude and appreciation for my father Abdullah Alyalak, my mother Khalidah Almane and my siblings for their unconditional love and support, which has always made me stronger.

Dedication

To my favorite person in the world, my best friend and my sister,

Shaikhah Alyalak

Table of Contents

List of Figures

List of Tables

Chapter 1 Block copolymer lithography

1.1 Introduction

Semiconductor industry is focusing nowadays on developing devices with minimum size by different upgraded lithographic techniques. As this demand is increasing, the top-down photolithography is reaching its limits in the continued drive to meet Moor's law.[1] Conventional photolithography has the capability of providing arbitrary pattern of light that has been projected through a pre-patterned photo-mask. [2] Having said that, Photolithography, even with state-of-art 193nm immersion technology with multi-patterning ability, is extremely hard to scale below 10nm. [1] One promising approach that has drawn scientists' attention is the use of block copolymer self-assembly in lithography. The block copolymer molecule assembles into periodic structure on the 10 to 100-nanometer length scale.[2] Not only it offers smaller feature size, but also it is easy to chemically alter the block copolymer or selectively remove one of the block copolymer components. In the past few years, interesting developments have been made on the use of block copolymers in many different areas including "covering the feature size, line-edge roughness, lateral ordering and etch contrast." The process of guided/directed self-assembly of block copolymers is an excellent candidate for devices fabrication to serve Moor's law for longer time. However, there are challenges that need to be conquered to reach this target. [1]

The nano-structure produced by block copolymer self-assembly is restricted to the periodic patterns created by the molecules of block copolymers; consequently, the block copolymers serve as templates. Different techniques are used to transfer the pattern, which is typically an array of lines or dots, into different types of materials. Many researchers benefit from this technology in developing ultra-dense memory devices, for example: FLASH memory chips and magnetic hard drives. [2]

This chapter focuses on interpreting the use of block copolymer self-assembly in nanolithography and the important factors affecting the self-assembly process. Also, the way the assembled morphologies can be modified and guided in thin films. Lastly, the different pattern transfer methods will be discussed.

1.2 Block Copolymer Self-assembly

1.2.1 Definition

"Self assembly is the process by which atoms, molecule, and/or components spontaneously organize into more complex object, shapes, and system." [3]

Block copolymers are sequences of chemically distinct macromolecules repeated units. AB block copolymers are a category of material developed from the polymerization of two different monomer types, which offers many interesting molecular structures. For example, when monomer A and monomer B undergo two-step polymerization process they form a basic structure called (A-B) diblock. Accordingly, (ABA) or (BAB) triblock copolymers form when three-step polymerization occur (Fig. 1.1). [4]

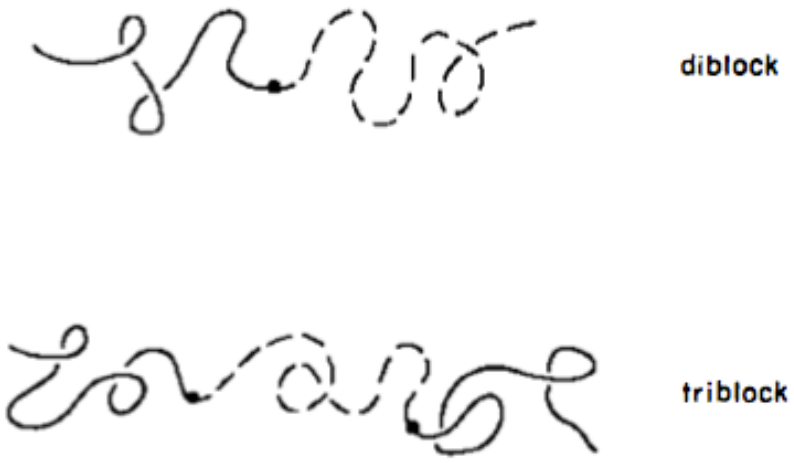

Figure 1-1 Demonstration of diblock and triblock copolymers. [4]

The structure of diblock copolymer might also be equivalent to AAAAAAAAAA-BBBBBBBB, as each block is homogenous and may reveal similar or dissimilar behaviors. [3]

So, "A block copolymer consists of two or more polymeric chains (blocks), which are chemically different and covalently attached to each other". [5] In the melt, they self assemble into a variety of structures as will be discussed in the following sections. This research focuses on diblock copolymers only, and BCP is used throughout this chapter to indicate block copolymers.

1.2.2 Controlling the BCP Self-assembly

The self-assembly process can be controlled by three experimentally adjustable factors: the degree of polymerization (N), the composition (f) (over all volume fraction of the A component) [4] and the A-B Flory-Huggins interaction parameter (x). All these factors affect the Gibbs free energy of the system (solution in this case) as described in the Flory-Huggins equation:

$$\frac{\Delta G_{\mathrm{mix}}}{k_{\mathrm{b}}T} = \frac{1}{N_{\mathrm{A}}}\ln\left(f_{\mathrm{A}}\right) + \frac{1}{N_{\mathrm{B}}}\ln\left(f_{\mathrm{B}}\right) + f_{\mathrm{A}}f_{\mathrm{B}}\chi \qquad \{1\}$$

The first two parts of the equation (N) and (f) correspond to the configurational entropy. So, by changing the polymerization chemistry, the relative length of the chain and the fraction of A to B polymer can be controlled. On the other had, the third term of the equation "(X) is associated with the non-ideal penalty of A-B monomer contacts and is a function of both the chemistry of the molecules and the temperature". Therefore, (X) is experimentally controlled by temperature. [5]

Due to the connectivity of the BCPs, the phase separation doesn't result in complete separation between the blocks, instead, the BCP chain arranges to have A and B segments on opposite sides of an interface. Therefore, "the equilibrium nano-domain structure must minimize unfavorable A-B contact without over-stretching the blocks", and the level of stretching corresponds to NX where N is the degree of polymerization and X is A-B Flory-Huggins interaction parameter. [5]

Different nano-structures can be formed by the self-assembly process when NX>10 (below order-disorder temperature ODT) (Fig. 1.2). When the volume fraction of the block A (fA) is small, it forms body-center cubic (BCC) lattice in B matrix. As the volume fraction of A increases, cylinders will form in hexagonal lattice, then a bicontinuous double gyroid structure, then finally lamellae. Accordingly, the shape of nano-domain depends on the volume fraction of one BCP to another; the size and periodicity of nano-domain depend on the total number of the units consisting of the BCPs (degree of polymerization), and X Flory-Huggins interaction parameter. [5]

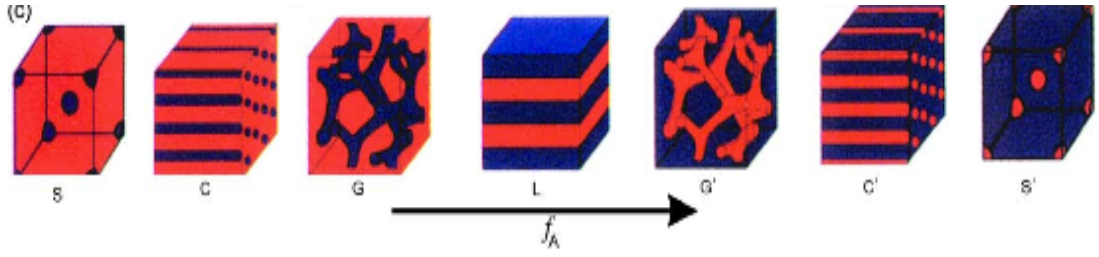

Figure 1-2 BCP self assembly into different shapes below the ODT, depends on the volume fraction, under the condition NX>10. [5]

1.3 Block Copolymer Thin Films

A common method for BCP thin films preparation is spin coating. This process requires a polymeric solution (~1% by weight) and a spinning substrate. Few drops are placed on the substrate and the spinning speed and time are adjusted to obtain specific thickness. However, many factors affect the quality of the produced BCP film, as discussed below. [5]

1.3.1 Non-equilibrium Effects

Non-equilibrium effects are associated with solvent choosing and preparation process. For choosing the solvent, the physical properties must be considered; some solvents are crystallizable solvents, which might affect the orientation of BCP self-assembly. Moreover, self-assembly process might occur during the casting process of solutions. For the preparation of the BCP thin film, the BCP is in liquid solution that needs to be spin coated on the substrate; few things need to be considered, for example the evaporation rate and volatility of the solution. [5]

The self-assembly process happens during annealing the film at high temperatures (more than 170C) (6) so the BCP reaches its thermodynamic equilibrium morphology, and the solvent will be removed. [5]

Non-equilibrium effects are also associated with the molecular weight of the BCP. “For applications requiring large domain spacing, extremely large molecular weights are necessary”. Complex morphologies form when the molecular weight of the BCP is large, this causes an increase in the kinetic barrier to thermodynamic equilibrium. Having said this, a group of scientists show that vapor annealing works best with large BCP molecular weight. In summary, non-equilibrium effects are corresponding to factors prior to the self-assembly phenomenon. [5]

1.3.2 Equilibrium Effects

Equilibrium effects are associated with factors in direct interaction with the self-assembly process of BCP in thin films, for example, the thickness of BCP thin film, domain spacing of the self-assembled nano-domain (which is associated with the molecular weight of BCP), annealing time and temperature and finally the surface energy of the substrate. All these factors are strongly affected by one another and equally important as explained in the following.

1.3.2.1 Confinement

Block copolymer thin films are subjected to a degree of confinement with the nanostructure domain spacing (L) and the film thickness (t). This research focuses on "soft confinement" in BCP thin films, where one interface is in direct contact with the atmosphere. In soft confinement, the stretching and compressing of a polymer chain "[are] mitigated by formation of islands or holes or by perpendicular orientation of the morphology (for cylinders and lamellae) depending on surface interactions". [6] In lamellar diblock copolymer, islands/holes form when the surface is preferential for one of the block copolymer, where nanostructures reorientations form when the surface is non-preferential "neutral". The degree of confinement or incommensurability is described by the ratio between t/L. The commensurability is achieved when t/L= n (n= 1,2,3..) and no islands/holes will be formed, which means the surface is neutral. When the surface is preferential to one block of the BCP, incommensurability is achieved when t/L= n+0.5.

For example, Figure 1.3 shows the different thicknesses of BCP PS-b-PMMA annealed at 170C. The molecular weight Mn for this BCP is 51 kg/mol, L= 27-30nm. [6]

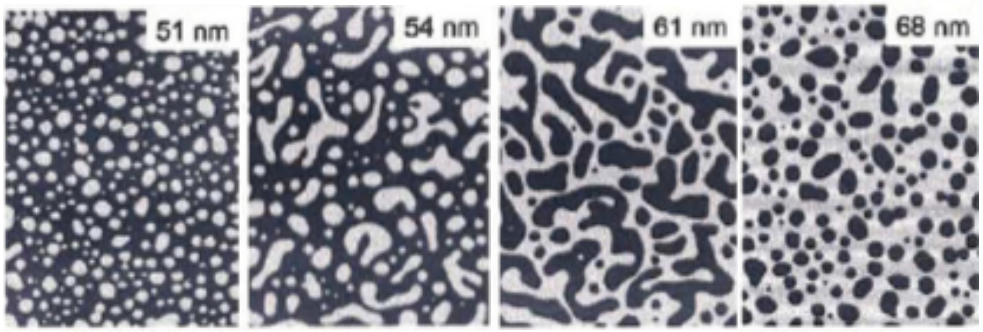

Figure 1-3 Lamellar PS-b-PMMA thin films, the morphology changes from islands to spindola island\hole structure with increasing the thickness of the film. Mn=51 kh\mol, L=27-30nm. When calculating the ration t/L for each thickness: (51/30)= 1.7, (54/30)= 1.8, (61/30)= 2, (68/30)= 2.2. [6]

For BCP with different symmetric structure than lamellar, for example cylindrical, calculating the commensurability conditions is more difficult. Cylindrical BCP forms spherical structure that can be arranged in a hexagonal array in very thin films (up to four layers of spheres), which increases the level of complexity as wetting, layer formation and surface reconstruction all affect the interaction between confinement and the surface of the substrate. [6]

1.3.2.2 Substrate Surface Effects

Although the thickness of BCP in thin films and the annealing conditions are very important factors in achieving high quality self-assembled BCP thin films, it is necessary to avoid any preferential wetting of the substrate by one block allowing the perpendicular structure to occur. This can be achieved by chemical modification of surface prior to spin coating of BCP. There are different chemicals and techniques used to neutralize the surface, as discussed in the following.

1.4 Directed Self-assembly of Block copolymer DSA

Directed self-assembly technology holds the potential for expanding the use of high-volume patterning of nano-electronic devices. This will enhance the functional density and diversification of electronic products at lower costs. To achieve this goal, an interdisciplinary knowledge of nano-scale patterning and assembly is required, for example nanofabrication methods and molecular self-organization. "Candidate materials for DSA processing tend to be considered for their potential to replace photoresist, as etch barriers. These materials include nanowires and nanotubes, graphene, dendrimers, phase-segregation block copolymers, and functionalized biomaterials, such as DNA and peptides." The most promising material for the near future applications is phase-segregation block copolymers, which is the focus of this research. Chemical patterning and e-beam lithography approaches to direct the self-assembly process of BCP will be discusses in the following. [3]

1.4.1 Definitions

"Directed self-assembly is process by which external factors, such as physical templates and/or fields, influence self-assembling systems in desired ways". [3] Two compatible methods were developed by researchers to achieve guided block copolymer features over large area: the grapho- and chemical- epitaxy approaches. [7]

Epitaxial self-assembly is the process of chemical templating of block copolymers on lithographically patterned monolayer. For example, "chemical modification of a substrate surface into hydrophobic and hydrophilic patterns can induce a diblock copolymer to phase segregate into similar patterns" as shown in Figure 1.4. [3]

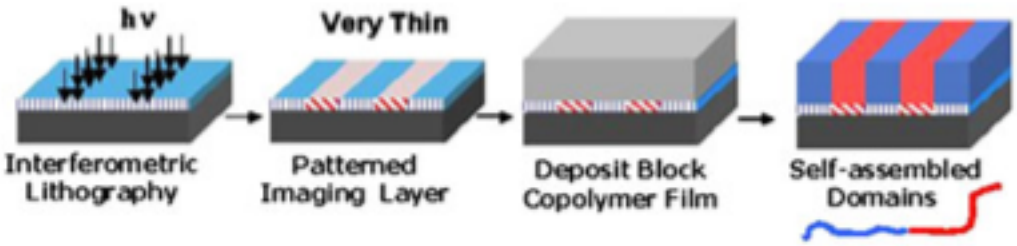

Figure 1-4 Epitaxial self-assembly of block copolymers on lithographically modified nnao-pattern substrate. [3]

Graphoepitaxy is the process that involves using conventional lithography (such as e-beam lithography) along with chemical treatment of the substrate to create the desired topographical structure to guide block copolymer self-assembly over a large area. The main challenge in this method is to have a stable graphoepitaxial pre-structured surface, which is resistant to solvent treatment and/or high temperatures needed for the BCP self assembly process. [7] Figure 1.5 shows schematic diagram of the process.

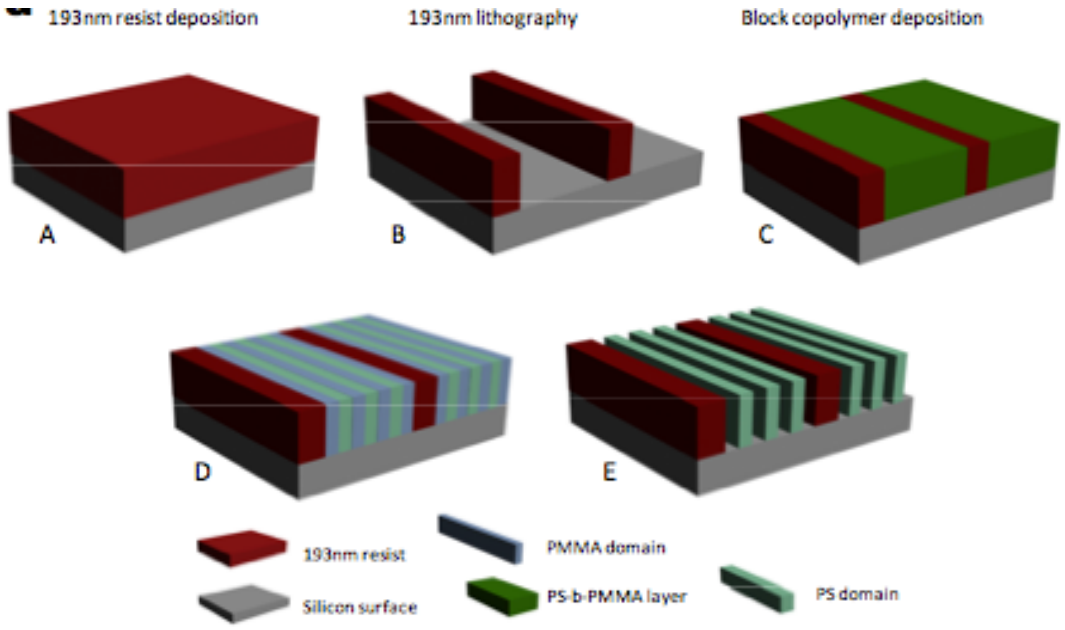

Figure 1-5 Summery of graphoepitaxy process (without the use of any chemical modifications). (a) Si substrate with 193nm resists (b) 193nm lithography (c) spin coating and annealing of BCP PS-b-PMMA (d) BCP self-assembly after thermal annealing (e) selective removal of PMMA. [8]

1.4.2 Defect Density

The greatest challenge of this technology might be controlling and understanding the defect density in DSA block copolymer system. The research target is <0.01 10nm defect/cm2, and a few data on chemically patterned substrates reported defect densities are ordered of a magnitude greater than the research target. For nanostructures that form through phase segregation of block copolymers, the equilibrium defects are relatively few and largely originate from kinetic effects arising during film growth or form the confinement of these materials when they are topographically directed". [3]

1.4.3 Directed Self-assembly of PS-b-PMMA

The research work presented in this thesis has been preformed using diblock copolymer PS-b-PMMA (poly (styrene) and poly (methyl methacrylate)), as this BCP is very popular due to its unique chemical and physical properties.

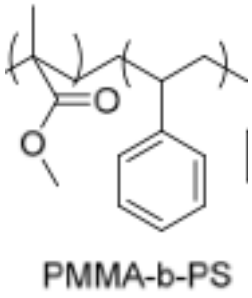

Figure 1-6 Chemical structure of PMMA-b-PS. [8]

PS-b-PMMA has a small Flory-Huggins interaction parameter (~0.043 at 25C) Table 1.1 below shows Flory-Huggins parameter for different BCPs.

Table 1-1 Flory-Huggins parameter for different BCPs. [1]

polymer name	χ at 25°C	χ at 180°C
PS-*b*-PMMA [57]	~ 0.043	~ 0.038
PS-*b*-PEO [58]	~ 0.077	~ 0.043
PS-*b*-PI [59]	~ 0.088	~ 0.050
PS-*b*-P2VP [60]	~ 0.178	~ 0.106
PS-*b*-PLA [61]	~ 0.217	~ 0.105
PS-*b*-PDMS [58]	~ 0.265	~ 0.187
PTMSS-*b*-PLA [62]	~ 0.478	~ 0.403
PS-*b*-PFS	n.a.	n.a.

As mentioned above, chemi-epitaxy or surface chemical modification and graphoepitaxy are the two major techniques to achieve guided self-assembled block copolymer domains. In the following section, these two techniques will be discussed for BCP PS-b-PMMA.

1.4.3.1 PS-OH Brush

A group of scientists present in their paper "Polystyrene as a brush layer for directed self-assembly of block co-polymers" [9] detailed steps on how to achieve guided self-assembled PS-b-PMMA by surface chemical modification along with lithography and oxygen plasma to create different wettability regions on a polymer brush grafted on the surface.

First Si substrate was activated for the grafting process by oxygen plasma treatment. Then a layer of PS-OH was spin coated on the substrate with a thickness of ~40nm (PS-OH dissolved in 1.5% toluene) as illustrated in Figure 1.7.

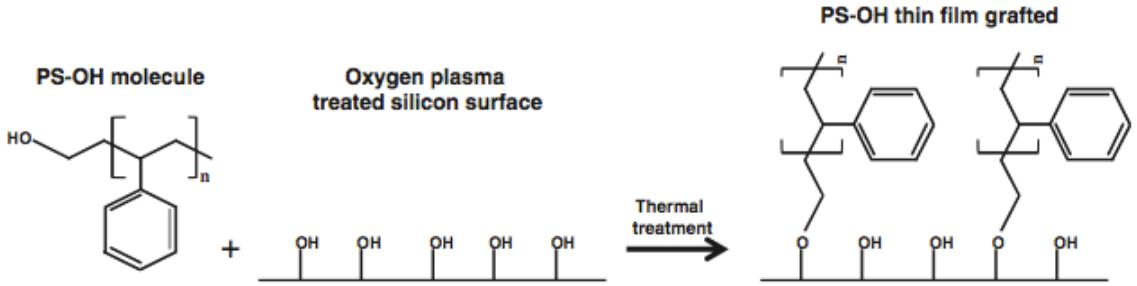

Figure 1-7 Polymer grafting process: reaction between PS-OH and silicon surface treated with oxygen plasma. [9]

To enable the terminal OH group to react with the native oxide layer, thermal treatment is preformed on the substrate after the spin coating of PS-OH layer. After the spin coating of PS-OH, two annealing conditions are preformed in order to make sure the reaction between OH on the surface and OH in the PS-OH happens. First, annealing is preformed inside a vacuum oven at 160C for 48h and the second annealing is at 195C for 2 minutes on a hot plate in ambient conditions (21C and 40 percent humidity). Then the samples are rinsed with toluene in ultrasound at 45C for 5 minutes to remove the polymer molecules that have not reacted with the surface. Accordingly, the hydrophilicity of the PS-OH film depends on the annealing process used (hydrophobic surfaces provide neutral surface to BCP self-assembly). Another way to tune the chemical properties of the surface is by exposing the grafted polymer to oxygen plasma.

Guiding patterns are produced for DSA for PS-b-PMMA by using oxygen plasma (to tune the chemical properties of the PS-PH brush) and lithography to draw defined lines/trenches.

After grafting of PS-OH on the surface of Si substrate, a 70nm thick layer of PMMA, 950 kg/mol is spin coated on top of the surface and patterned by electron beam lithography. "Selected areas are exposed at 20 kV electron beam acceleration voltage with 20 µm column aperture and with a dose of 225 µC/cm^2. The width of the exposed areas is designed to range from 155nm to 465nm and the length is fixed to 25 µm ". [10] After development, the exposed parts of PS-OH brush are treated with oxygen plasma to change the chemical properties. The remaining resist layer is washed away with toluene leaving the surface with PS-OH layer with modified and un-modified areas (Figure 1.8). [9]

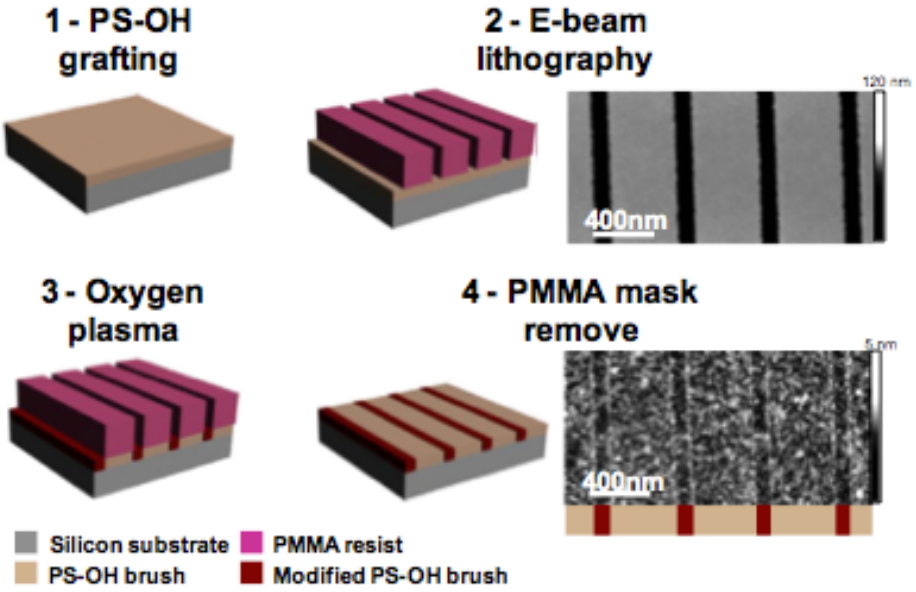

Figure 1-8 Steps to achieve different hydrophilicity areas on the same sample. AFM images on the right show the morphology of the surface. The top one is for the surface after two steps, and the bottom one after the fourth step. [9]

The BCP is ready to be deposited by spin coating on the surface (~57 nm thickness), then annealed to self-assemble at 190C for 20 minutes. However, prior to spin coating the surface with BCP, different oxygen plasma recipes (to tune the hydrophilicity of the exposed areas) are tested to achieve the best results for guided PS-b-PMMA nano-structure. Figure 1.10 shows the final PS-b-PMMA self-assembly results after removing PMMA component, on PS-OH brush with different thermal annealing and oxygen plasma treatment. Figure (9-a) shows the guided pattern for the surface that has the brush annealed in the vacuum oven at 160C/48h, and oxygen plasma at 300w/50 scccm O2 for 10 seconds, whereas figure (9-b) shows the guided pattern for the surface that has the brush annealed on a hot plate at 195C/2min and oxygen plasma at 150w/20 scccm O2 for 20 seconds.

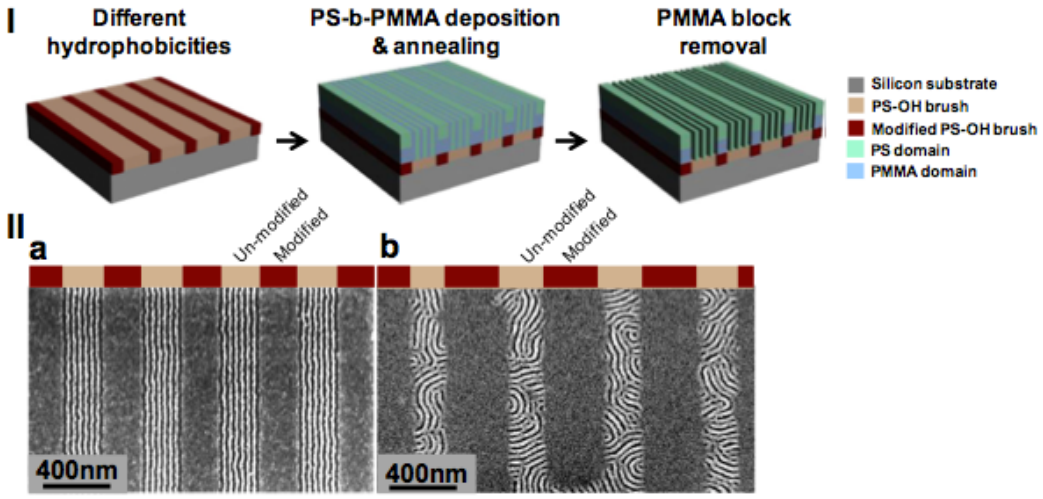

Figure 1-9 "process steps for alignment of PS-b-PMMA BCP using chemical surface modification" SEM images of the results of the BCP guided alignment after PMMA block removal using different process conditions" [9]

1.4.3.2 Grapho-epitaxial DSA Using HSQ

In grapho-epitaxy method, BCP self-assemble on a substrate with specific topography obtained by conventional lithography. The orientation of the self-assembled BCP depends on the surface energy of the substrate. [8]

Therefore, the surface substrate has to be neutral to PS-b-PMMA before preforming any lithography process to obtain certain topographical features. This is achieved by spin coating a random block copolymer PS-r-PMMA. When the surface is neutral, a layer of hydrogen silsesquioxane HSQ is deposited and e-beam writing creates a pattern on the surface. After PS-b-PMMA is spin-coated and self-assembled on the surface, a selective removal of PMMA by reactive ion etching is preformed (Fig. 1.10). [10]

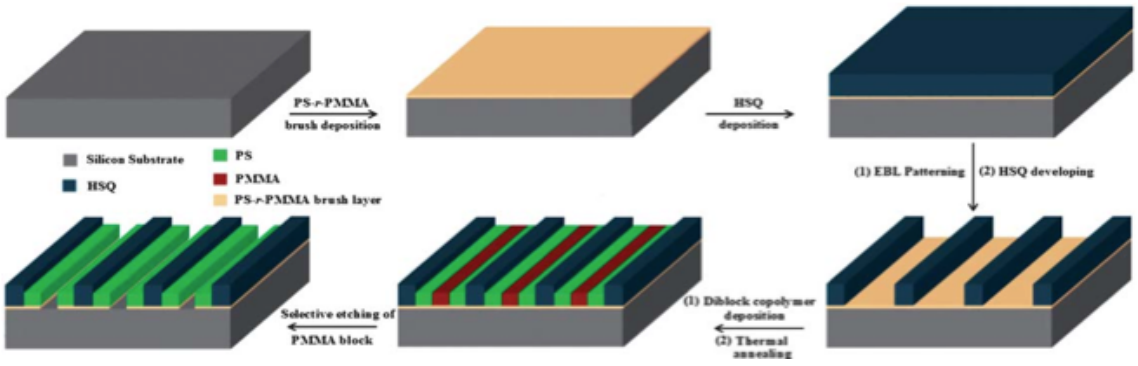

Figure 1-10 Steps of DSA for PS-b-PMMA by grapho-eptaxial approach using e-beam writing on HSQ resist. [10]

1.4.3.2.1 Random Copolymer

Copolymer consists of two monomers A and B with a random ordering in the polymeric chain. [3] A famous example is the random copolymer PS-r-PMMA as a very beneficial method to achieve perpendicular orientation of thermally self-assembled PS-b-PMMA. This random polymer is usually spin coated on a silicon substrate (100nm thick) then baked at 170C for 6h so the bond between the surface silanol and the copolymer hydroxyl function is formed. The un-grafted materials are then washed leaving the surface hydrophobic because of the styrene component on the surface. Therefore, by adjusting the chemical composition of the random copolymer brush, the wettability on the surface can be controlled to have the optimum interfacial interaction between the random

copolymer and BCP. After that, the BCP PS-b-PMMA is spin coated on the treated silicon substrate (~50nm) and placed on a hot plate as the self-assembly takes place at high temperature for a certain time (3 hours in vacuum at 180C in this example). Following that, to reveal the self-assembled pattern, one of the BCP is removed (PMMA in this case) by oxygen plasma. [7] Figure 1.11 shows AFM, TEM and SEM images for PS-b-PMMA pattern self-assembled on a modified surface by PS-r-PMMA brush. [3]

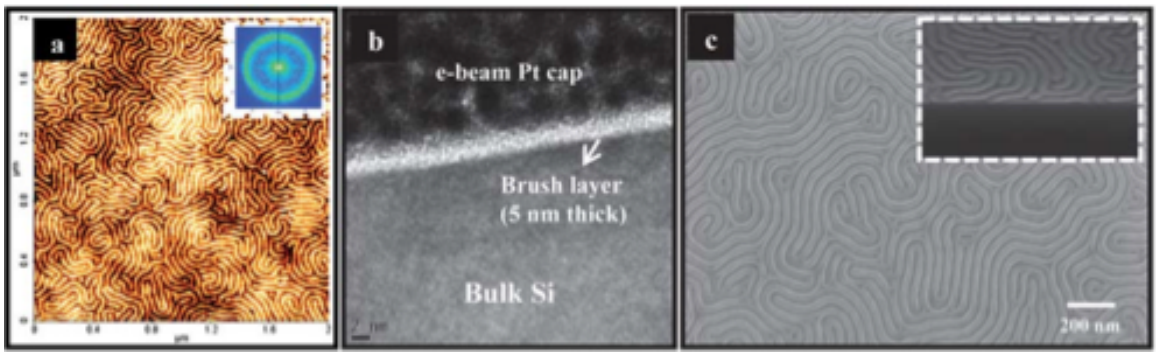

Figure 1-11 (a) AFM images of self-assembled PS-b-PMMA on Si surface modified by PS-r-PMMA brush (dark area is PMMA and brighter area is PS). (b) Shows TEM cross-section image of the brush layer (the bright area) on top of it is PS-b-PMAA film. (c) Top-view and inset SEM images of PS-b-PMMA film after select removing of PMMA by oxygen plasma, leaving the surface with PS lines (light gray lines). [10]

Following that, HSQ is spin-coated on the neutralized surface (~50nm thick) and e-beam writing process is done with the following parameters: exposed area 10x10 μm, width of the line 20nm, pitch period 100nm, e-beam exposure 1.4 mc.cm-2. After that, to reveal the pattern an aqueous solution mixture of NaOH and NaCl is used as a developer for 20 seconds. PS-b-PMMA is spin-coated (~43nm) and self-assembled after thermal treatment for 3hours in vacuum at 180C. Following that, PMMA is selectively removed by RIE using oxygen and argon. The directed self-assembly of PS-b-PMMA is achieved using this method (Fig. 1.12).

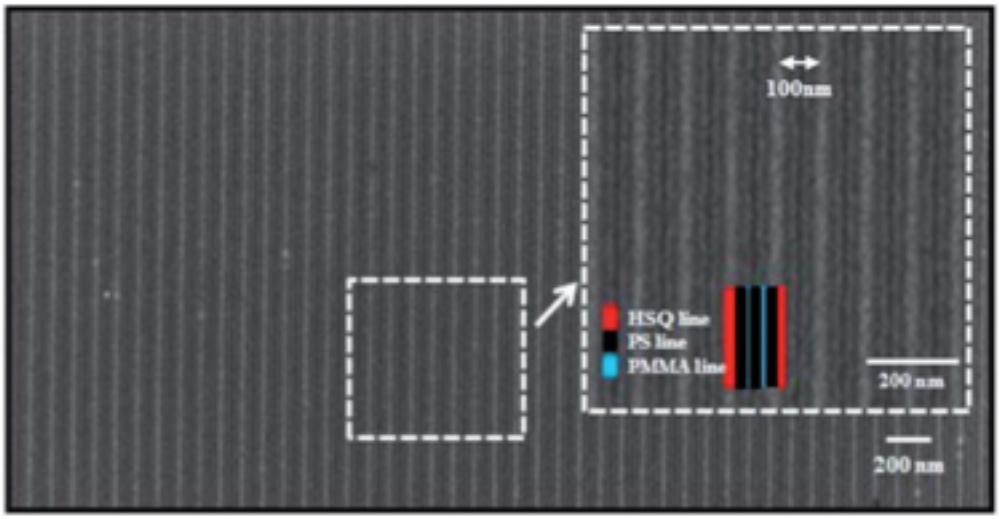

Figure 1-12 DSA of PS-b-PMMA on narrow HSQ gratings, light gray lines are HQS and dark ones are PS. [10]

1.5 Pattern Transfer

In conventional lithography, like photolithography, a layer of photoresist is spin-coated on the substrate. Then by shinning UV light through pre-patterned mask on the substrate and developing it afterwards, the pattern is now on the photoresist layer. To transfer the pattern to the substrate (Si usually), methods like reactive ion etching RIE or lift-off processes are used. [2]

In block copolymer lithography, a thin layer of BCP is spin-coated on the substrate, functioning as photoresist, in this case the pattern is produced by the self-assembly of BCP into one of its equilibrium phases (i.e. lamella or cylinder) rather than projecting UV through mask. The same pattern transfer methods are used in BCP lithography. [2] Figure 1.13 below shows pattern transfer using BCP lithography; the self-assembled process is obtained by using PS-OH brush. Oxygen plasma is used to selectively remove PMMA component and PS-OH brush, C2F8 and O2 are used to remove the polymer and finally SF6 is used to etch the silicon. [9]

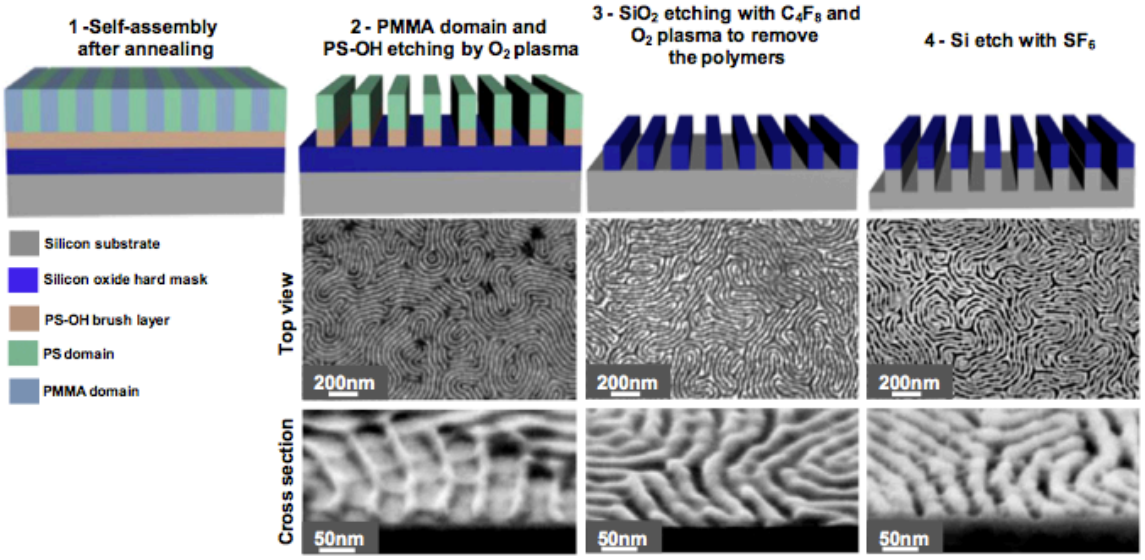

Figure 1-13 Pattern transfer of PS-b-PMMA using RIE, SEM images for each step. [9]

1.6 Conclusion

The use of block copolymers in lithography is rapidly developing, born out of a necessity when great challenges are faced with conventional lithography. The growing need of smaller feature size on the nano-scale requires exceptional time and effort using conventional lithography. Block copolymer lithography offers attractive and economical alternatives for researchers looking for smaller periodic patterns over large areas.

Scientists predict that the future of this technology will continue to evolve fast along with the techniques used to obtain the desired patterns. For example, long range ordering of BCPs will improve and new methods for selective removal of one component will be developed as the chemistry of BCPs are developing.

Chapter 2 PMMA-b-PS self-assembly

2.1 Introduction

Block copolymer lithography holds a great potential for applications in nanofabrication due to its ability to self-assemble into periodic structure on the tens of the nanometer length scale. As presented in the previous chapter, the size and morphology of the self-assembled nano-domain is controlled by the molecular weight and composition of the BCP. Thereby, the use of block copolymer lithography to achieve nano-structure over a large area, along with other nanofabrication techniques, is relatively easy. [11]

Researchers and scientists have spent a lot of time and effort studying symmetric diblock copolymer with lamellar nano-domains in order to fully understand the behavior of diblock copolymer in thin films. The orientation of the self-assembled nano-structure over a large area is very important to achieve functional pattern. The lamellar structure is oriented parallel to the substrate when "the relative interfacial energies between each block and the substrate, and the relative surface energy of each block induce a preferential wetting of one block at an interface". [11] Therefore, the surface energy of the substrate must be tuned or modified to have neutral surface in order to achieve a perpendicular orientation of the self-assembled pattern. Researchers have developed methods to neutralize the surface substrate prior to self-assembly of PS-b-PMMA, for example, grafting random block copolymer PS-r-PMMA of varying PS and PMMA component. However, this method is not cost-efficient and requires a very long time.

This chapter discusses the perpendicular lamellar nano-domain of symmetric PS-b-PMMA in thin films. This is achieved by vapor deposition of 3-(p-methoxyphenyl)propyltrichlorosilane (3-MPTS) prior to the self-assembly of PS-b-PMMA.

For this research, the used PS-b-PMMA is purchased from Polymer Source Inc.; it is symmetric with molecular weight 130 kg/mol. The solution is prepared by mixing

0.32g of PS-b-PMMA in 27ml Toluene. Also, an attempt to achieve a guided self-assembly process is reported.

The final obtained nano-domain is characterized by scanning electron microscope (SEM) and atomic force microscope (AFM). Both methods are capable of providing clear image of the PS-b-PMMA after a selective removal of PMMA with oxygen plasma.

2.2 Unmodified Surface

2.2.1 First Trial

The first attempt to get self-assembled pattern using PS-b-PMMA (~50nm) was done on an unmodified substrate, prior to spin-coating PS-b-PMMA, the samples were cleaned by solvents (acetone and IPA) only. The self-assembly process took place at an elevated temperature of 222C and the annealing time was as follows: 10min, 20min, 40min, 60min and 120min, and the process took place on a hot plate in the air. After that, PMMA was selectively removed using RIE with this recipe: RF power: 20W, pressure 20 mTorr, O2 flow rate 20 sscm for 15 seconds. SEM images below show the final results.

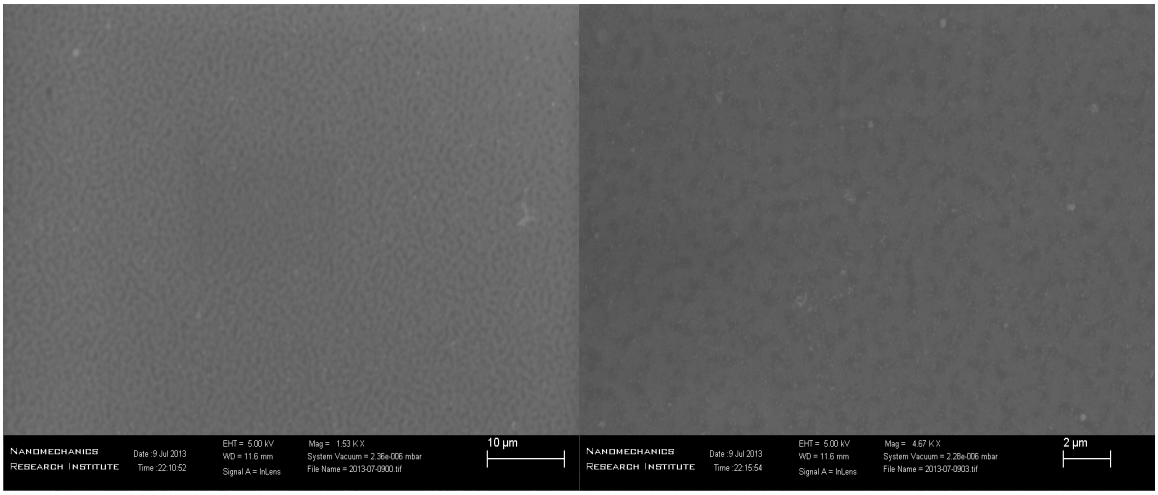

Figure 2-1 Self-assembly of PS-b-PMMA at 222C for 10min after removing PMMA

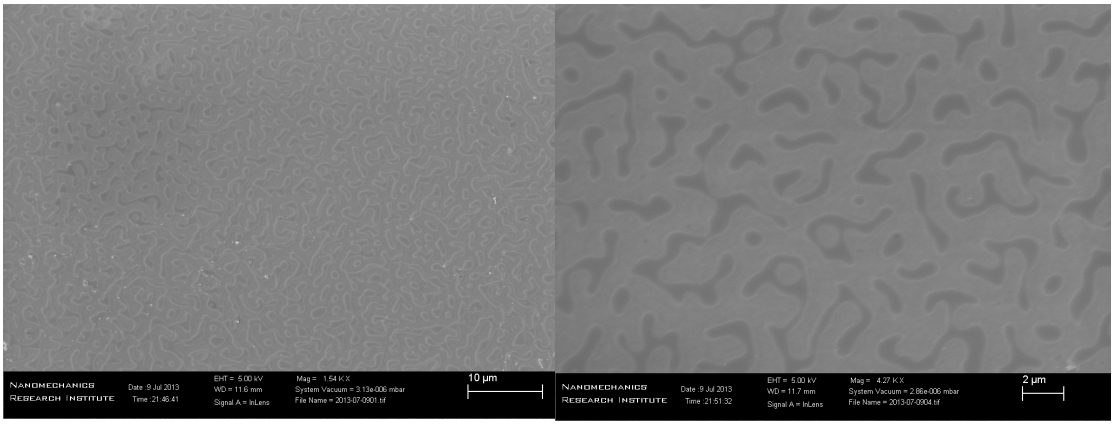

Figure 2-2Self-assembly of PS-b-PMMA at 222C for 20min after removing PMMA

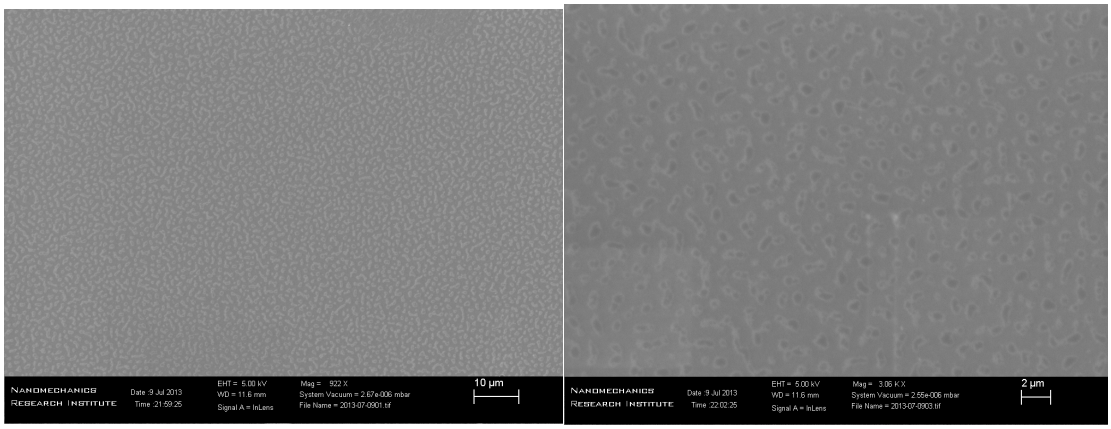

Figure 2-3Self-assembly of PS-b-PMMA at 222C for 40min after removing PMMA

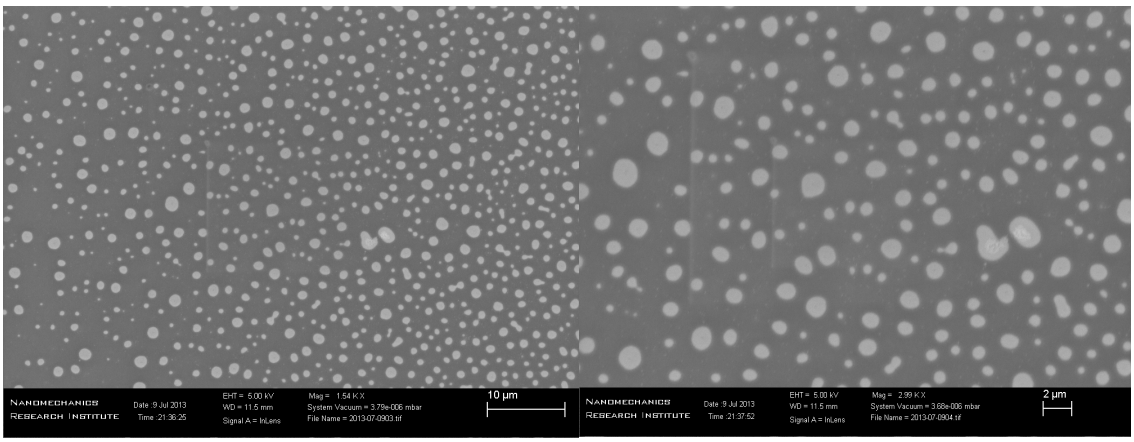

Figure 2-4Self-assembly of PS-b-PMMA at 222C for 60min after removing PMMA

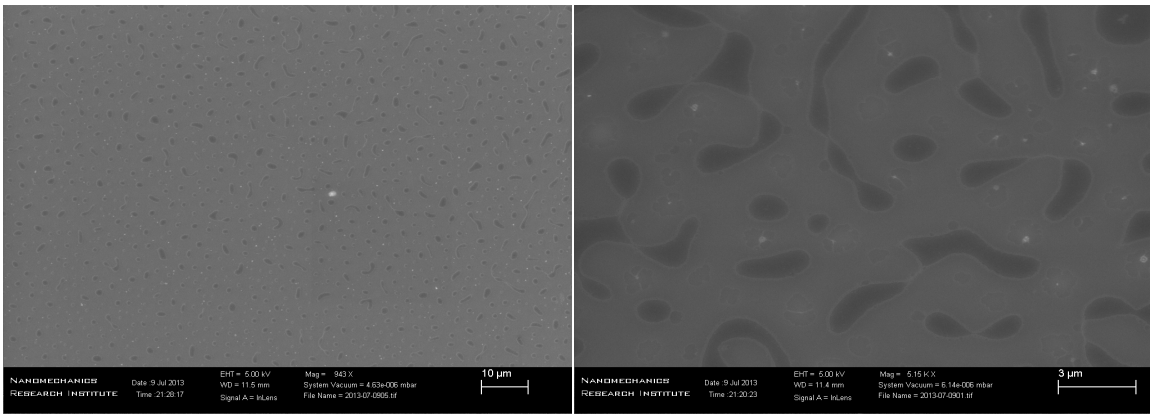

Figure 2-5 Self-assembly of PS-b-PMMA at 222C for 120min after removing PMMA

The SEM images show that PS-b-PMMA formed islands/holes due to preferential wetting toward one component (PMMA) (figure 2.6). Furthermore, based on the confinement conditions discussed on chapter one, SEM images show that the thickness of these 5 samples was not the same for every trial, as every image shows different configuration.

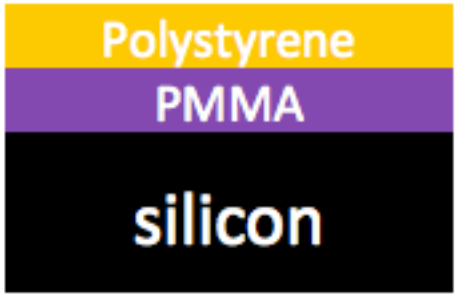

Figure 2-6 layer-by-layer configuration.

2.2.2 Second Trial

The second trial was done with changing all the parameters, annealing temperature, annealing time and the RIE time. One important factor of this trail is that the annealing process was done in a nitrogen box. After cleaning the samples with solvent and oxygen plasma, PS-b-PMMA was spin coated on the substrate (~55nm) and left on a hot plate at 190C for 3,8 and 20 minutes inside a nitrogen box. Following that, RIE was preformed to remove PMMA, using this recipe: RF power 20W, pressure 1 mTorr, O2 flow rate 20 sscm for 26 seconds. SEM images below show the final results.

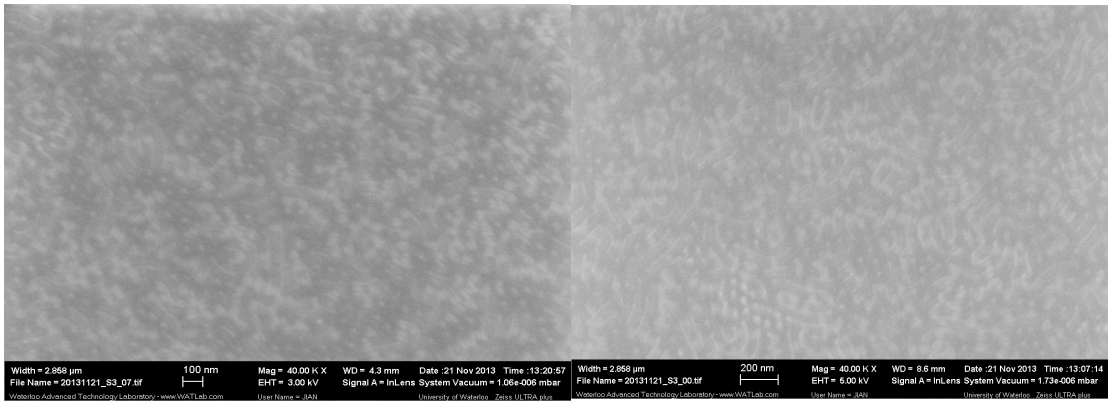

Figure 2-7 Self-assembly of PS-b-PMMA at 190C for 3min after removing PMMA

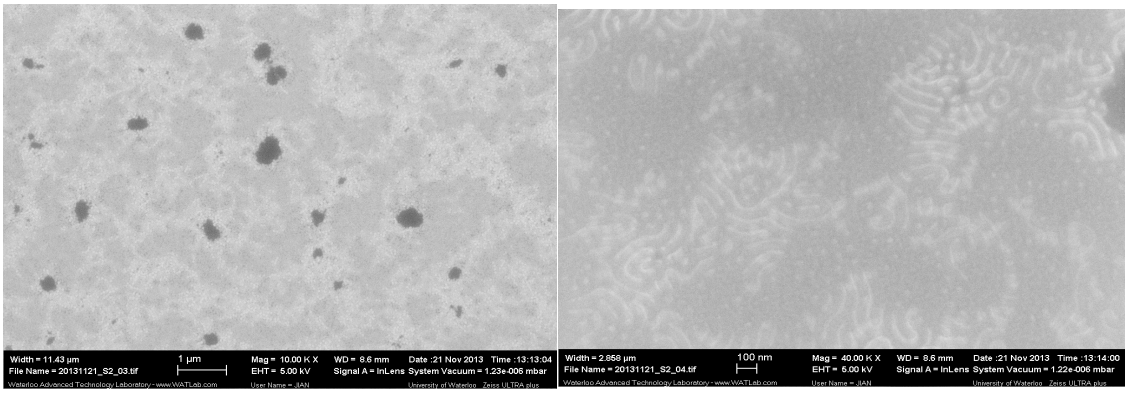

Figure 2-8 Self-assembly of PS-b-PMMA at 190C for 8min after removing PMMA

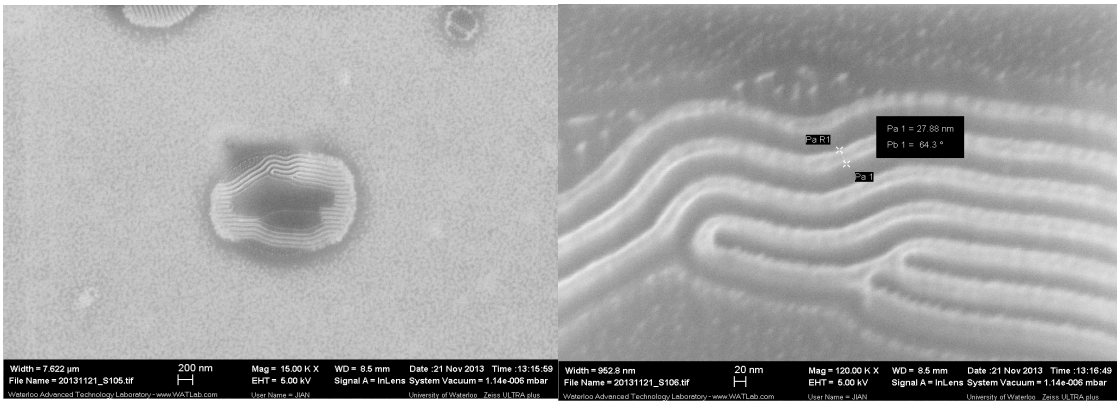

Figure 2-9 Self-assembly of PS-b-PMMA at 190C for 20min after removing PMMA

For the samples annealed for 3 and 8 minutes, the discontinuity of the pattern along with the mixture of island and holes indicate that commensurability was not achieved. Also, the orientation of the pattern is parallel to the substrate (figure 2.6). The sample annealed for 20mins showed an interesting pattern, it is clear form the SEM images (figure 2.9) that there is a perpendicular/standing pattern of PS (PMMA was removed by RIE). However, this perpendicular nano-domain was not covering the whole substrate.

2.2.3 Third Trial

In an attempt to achieve a perpendicular pattern covering the whole surface, the same process in the second trail was repeated with changing one parameter only, which is the etching time (12Seconds).

So, for this trial three samples were cleaned with solvents (acetone and IPA) and oxygen plasma. The PS-b-PMMA was spin-coated on the substrates and left on a hot plate at 190C inside nitrogen box for 3,8 and 20 minutes to self assemble. Following the annealing process, PMMA component was removed using RIE. SEM images below show the final results.

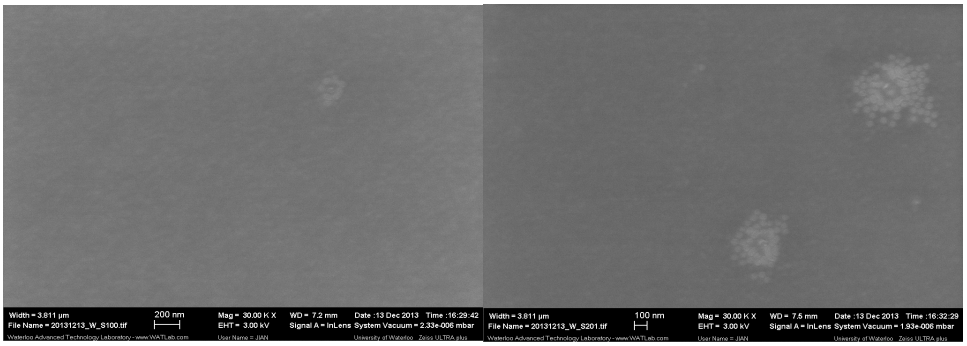

(a) (b)

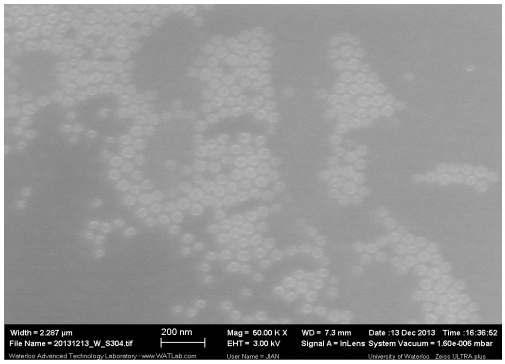

(c)

Figure 2-10Self-assembly of PS-b-PMMA at 190C for a) 20min b) 8min c) 3min after removing PMMA

2.3 Modified Surface Prepared by Vapor Phase Coating

The results for the self-assembly process on an unmodified surface show that the oritation of the nano-domains is parallel to the surface (layer-by-layer configuration). Although for the second

trial the sample annealed at 190C for 20min showed perpendicular nano-domain, it was discontinued and not covering the whole surface.

In order to achieve a continuous perpendicular nano-domain by PS-b-PMMA self-assembly, the surface must be neutral to both PS and PMMA. One interesting way to achieve this is by depositing 3-(p-methoxyphenyl)propyltrichlorosilane (3-MPTS) by liquid phase as reported by B.H. Sohn and S.H. Yum in their paper "Perpendicular lamellae induced at the interface of neutral self-assembled monolayers in thin diblock copolymer films". [11] This method provides satisfying results; however, a long time is required to deposit 3-MPTS (48hours) (figure 2.11)

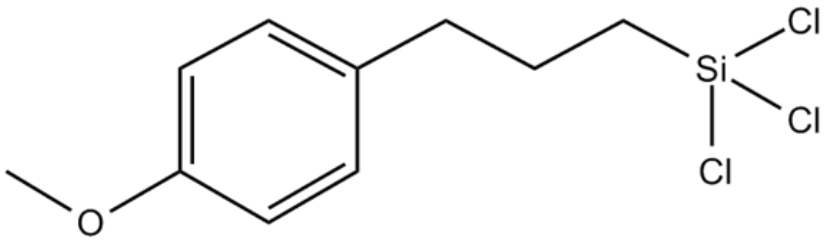

Figure 2-11 Chemical structure of 3-MPTS

As PMMA has a higher surface energy, it always prefers polar native oxide layer (SiOx/Si), this is the reason self-assembly of PS-b-PMMA over untreated surface gives parallel structure. However, depositing a very thin layer of 3-MPTS will tune the surface energy. What is unique about 3-MPTS is its chemical structure, it "has a similar functional head structure (p-methoxyphenyl group) to poly(phenylene oxide)", which is a miscible polymer with PS homopolymers figure (2.11). This tunes the surface energy of the substrate, as PS has naturally lower surface energy than PMMA, leaving the surface neutral without any preference to one block. [11]

In this research, 3-MPTS was also used to neutralize the surface substrate, but instead of using liquid phase deposition, vapor phase deposition was used. It is achieved by placing one drop of 3-MPTS in a wafer box then leaving the substrate inside this wafer box for two hours on a hot plate (no vacuum).

2.3.1 Vapor Deposition of 3-MPTS at High Temperatures

The process of the vapor deposition was preformed on four different temperatures 90C, 100C and 130C. Following that, PS-b-PMMA was spin coated on the four treated samples, then annealed on a hot plate inside a nitrogen glove box at 190C for 20 minutes. And oxygen plasma using RIE was preformed to remove PMMA component, the recipe used is: RF power 20W, pressure 1 mTorr, O2 flow rate 20 sscm for 12seconds AFM and SEM images below show the final results.

2.3.1.1 Vapor Deposition of 3-MPTS at 90C for 2h

After the vapor deposition of 3-MPTS at 90C for two hours, PS-b-PMMA was spun-coated over the samples (~80nm). The annealing was done in a hot plate inside a nitrogen glove box at 190C for 3min, 8min and 20min. AFM images below show the final results.

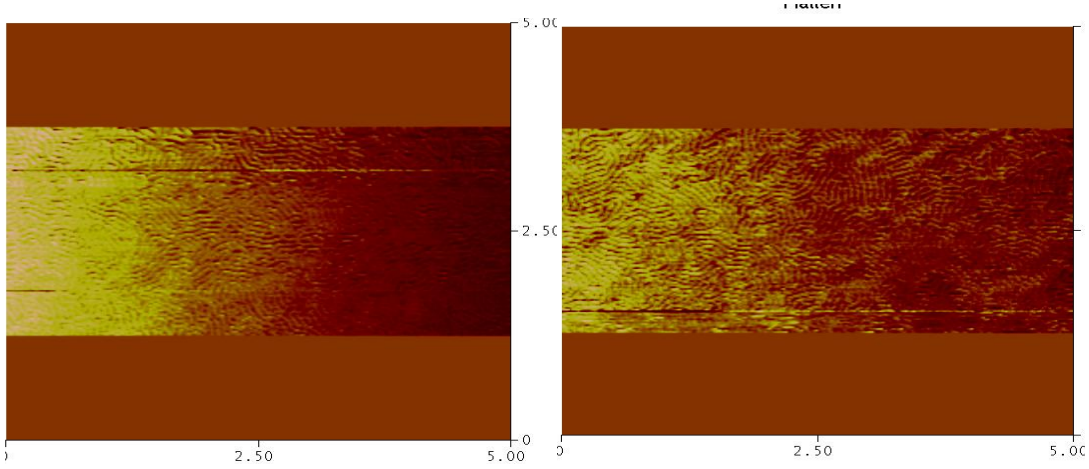

(a) (b)

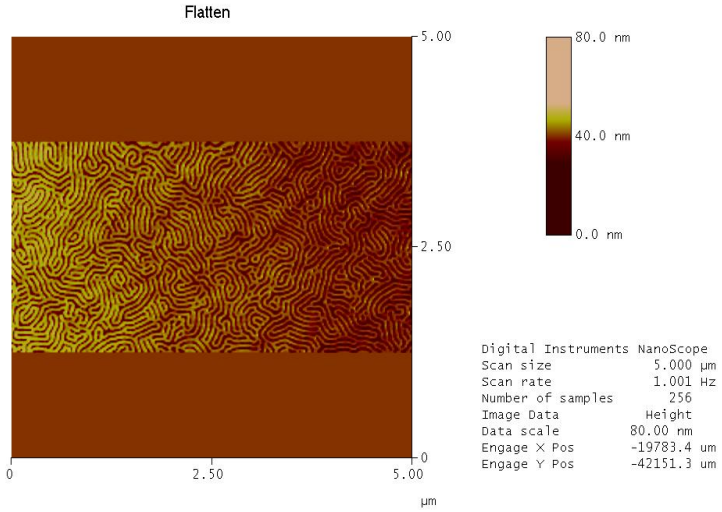

(c)

Figure 2-12 Self-assembly of PS-b-PMMA ~80nm over treated surface with 3-MPTS at 90C for 2h, a) annealing of BCP for 3min at 190C b) annealing of BCP for 8min at 190C c) annealing of BCP for 20min at 190C after removing PMMA.

As expected, after removing the PMMA component, AFM images show the self-assembled perpendicular structure over the whole surface. The annealing time for self-assembling PS-b-PMMA has also affected the final pattern. Films annealed for 3 and 8 minutes did not give good quality patterns, however, annealing BCP for 20minuts provided a satisfactory finger print pattern. Therefore, for the following trials the self-assembly annealing time for PS-b-PMMA is only 20min at 190C in the nitrogen glove box.

2.3.1.2 Vapor Deposition of 3-MPTS at 100C for 2h

The same vapor deposition process was repeated on higher temperature, 100C for 2h. Then PS-b-PMMA was spin coated (~120nm) then annealed for 20min at 190C in a nitrogen glove box (figure 2.13).

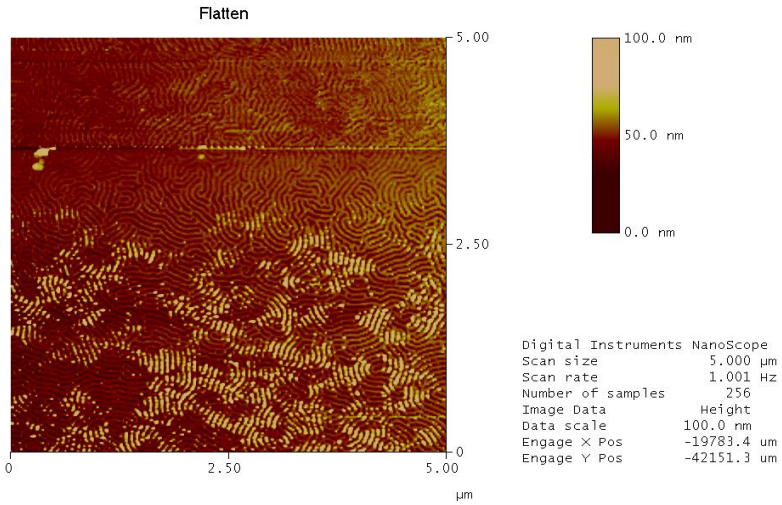

Figure 2-13 Self-assembly of PS-b-PMMA ~120nm over treated surface with 3-MPTS at 100C for 2h, annealing of BCP for 20min at 190C after removing PMMA.

2.3.1.3 Vapor Deposition of 3-MPTS at 130C for 2h

The same vapor deposition process was repeated on a higher temperature, 130C for 2h. Then PS-b-PMMA was spin coated (~135nm) then annealed for 20min at 190C in a nitrogen glove box. Figure 2.14 shows the final pattern after the selective removal of PMMA with oxygen plasma with the same recipe mentioned above.

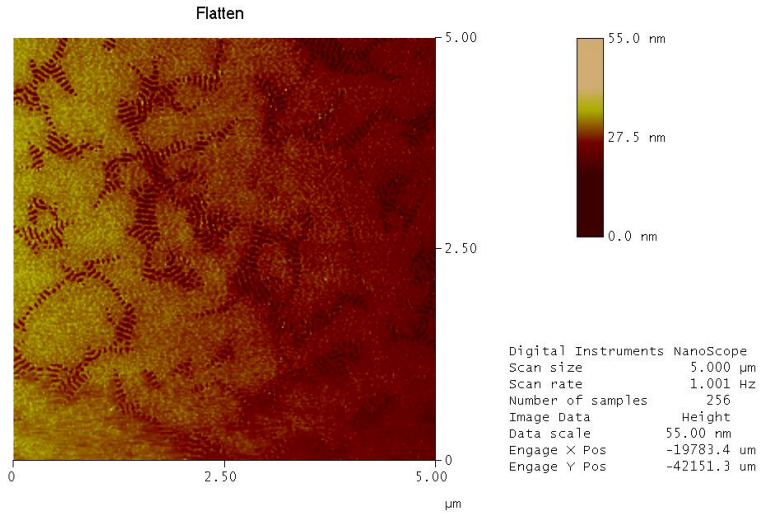

Figure 2-14Self-assembly of PS-b-PMMA ~135nm over treated surface with 3-MPTS at 130C for 2h, annealing of BCP for 20min at 190C after removing PMMA.

AFM images show that the vapor deposition of 3-MPTS on high temperatures does not provide a good surface for PS-b-PMMA to self-assemble on. Also, the higher the temperature is, the more of 3-MPTS will be deposited on the substrate leaving the surface with relatively thick layer of 3-MPTS (~1.3nm of 3-MPTS is ideal). [11]

2.3.2 Vapor Deposition of 3-MPTS at Room Temperature

Based on the presented results, vapor deposition of 3-MPTS on lower temperatures provides a better surface for PS-b-PMMA to self-assemble on. Therefore, the process of 3-MPTS vapor deposition was done at room temperature (20C) for 2hours without the use of hot plate. PS-b-PMMA was then spin coated and annealed for 20minutes on 190C-hot plate inside a nitrogen box. The same process of removing PMMA with RIE was applied.

AFM and SEM images show the final pattern assembled on surface treated with 3-MPTS by vapor deposition in room temperature. (Figure 2.15) & (figure 2.16).

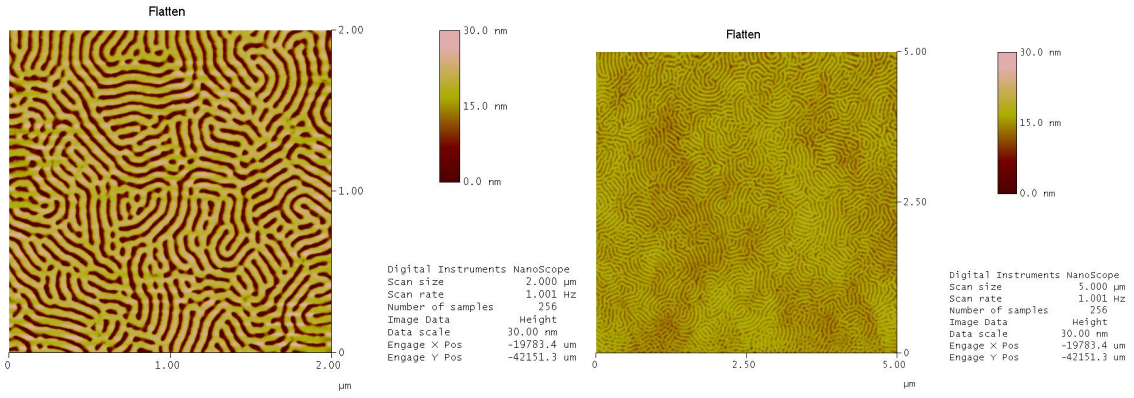

Figure 2-15AFM images of Self-assembled PS-b-PMMA ~450nm over treated surface with 3-MPTS at room temperature 20C for 2h, annealing of BCP for 20min at 190C after removing PMMA.

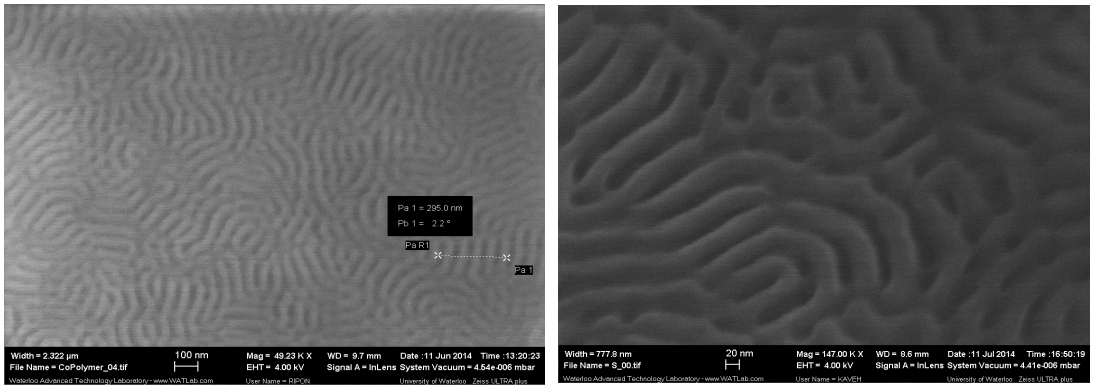

Figure 2-16 SEM images of Self-assembled PS-b-PMMA ~450nm over treated surface with 3-MPTS at room temperature 20C for 2h, annealing of BCP for 20min at 190C after removing PMMA.

AFM and SEM images show that PS-b-PMMA self-assembled into a perpendicular fingerprint pattern all over the substrate. However, the thickness of the PS-b-PMMA ~450nm is quite thick and using thinner films is more beneficial. Therefore, the same process was repeated using two different thicknesses of PS-b-PMMA 130nm and 90nm (figure 2.17).

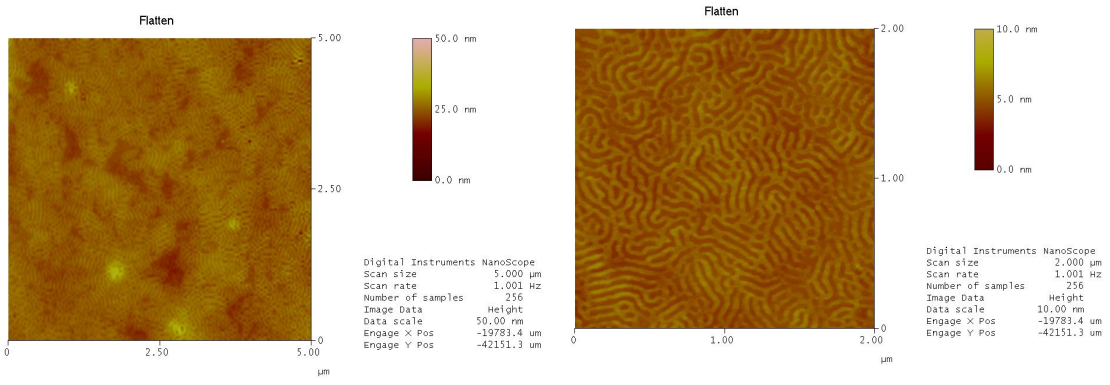

(a) (b)

Figure 2-17AFM images of Self-assembled PS-b-PMMA over treated surface with 3-MPTS at room temperature 20C for 2h, annealing of BCP for 20min at 190C after removing PMMA. a) PS-b-PMMA thickness ~90nm. b) PS-b-PMMA thickness ~130nm

Depending on the presented results, coating the silicon substrate with a monolayer of 3-MPTS (~1.3nm) [11] tunes the surface energy of the substrate, which prevents any preferential wetting for one component. As a results, PS-b-PMMA self-assemble into perpendicular pattern covering the whole substrate.

The process of depositing 3-MPTS was done by vapor deposition of the chemical at room temperature for 2 hours without the use of vacuum or hot plate. Also this method provides perpendicular self-assembled PS-b-PMMA pattern regardless of the thickness of BCP film.

2.4 Guided Self-assembly of PS-b-PMMA

Guiding the self-assembly process of PS-b-PMMA to produce desired patterns with small features is crucial to the industry. As presented in the previous chapter, there are few methods to direct the self-assembly process of PS-b-PMMA and they usually involve the use of conventional fabrication methods, such as, pre-patterning the surface with e-beam lithography (EBL) then neutralizing the surface to have a perpendicular orientation.

In this research, an attempt to guide the self-assembly process has been made using EBL and 3-MPTS as it is discussed below.

2.4.1 DSA by EBL Using PS resist

In this process, a layer of Polystyrene PS was spin coated on the surface and patterned by using e-beam lithography. Following that, 3-MPTS was deposited on the surface by vapor deposition (for 2h at 20C) to neutralize the surface energy for PS-b-PMMA (figure 2.18)

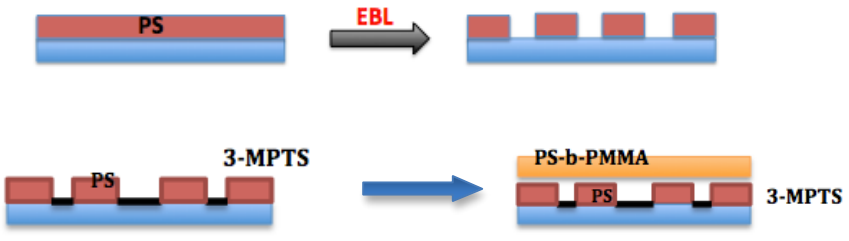

Figure 2-18 Schematic diagram of DSA for PS-b-PMMA using EBL.

The guiding patterns were created for DSA of PS-b-PMMA using the following process steps: PS was spin coated on Si substrate and patterned by EBL, selected areas were exposed to 20 kV electron beam voltage with a 30 µm column aperture and with a dose area from 100 to 12800 cm/cm2, and 12nm center-to-center and line spacing 12nm. The line doses were designed to range from 1 to 128 nc/cm with 6nm center-to-center and line spacing of 52nm (figure 2.19)

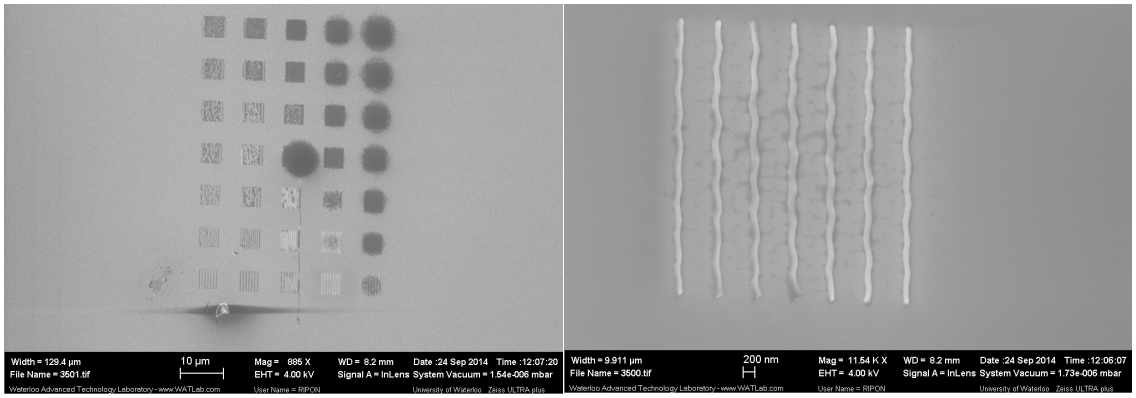

(a) (b)

Figure 2-19 (a) Pattern produced by EBL on layer of PS (b) zoom in to a low dose line pattern.

Following that, 3-MPTS was deposited on the substrate via vapor deposition for 2h at 20C. PS-b-PMMA was then spin coated ~70nm and annealed for 20minutes on a 190C-hot-plate inside a nitrogen box. After the annealing process, PMMA was removed by RIE with the same recipe mentioned previously. SEM images show the final results figure (2.20)

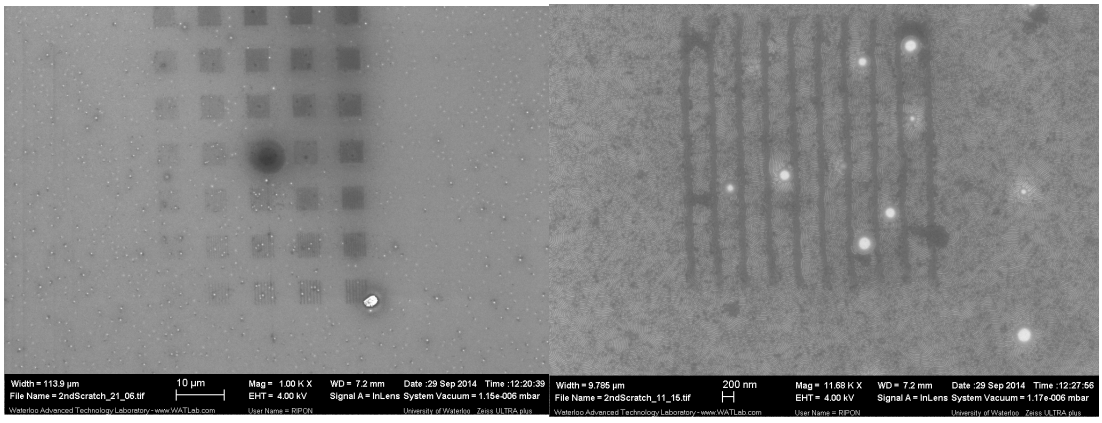

(a) (b)

Figure 2-20 (a) Pattern produced by EBL after spin-coating and annealing of PS-b-PMMA (b) zoom in to a low dose

SEM images show the self-assembled pattern, however it was not guided. The PS pattern that was created by EBL did not help the self-assembled pattern to be guided between the PS lines.

2.5 Conclusion

This chapter has shown an easy and fast way to achieve a perpendicular self-assembled pattern of PS-b-PMMA. It depends on neutralizing the surface using 3-MPTS by vapor deposition for 2h at room temperature. Results show that the self-assembled pattern is covering the whole sample, which is always desirable.

The guided self-assembly process was not successful using the mentioned method, however, improvements can be done on future work.

Chapter 3 Graphene Electronics

3.1 Introduction

Graphene, a two-dimensional sheet of carbon atoms, fabricated through micromechanical cleavage of graphite crystal, was first produced in the lab in 2004. [12,13] Since then, graphene has been one of the most interesting materials due to its exceptional physical, chemical and electrical properties, such as mechanical strength and high mobility, [13] which makes graphene an excellent candidate to replace silicon in different electronic applications like super-capacitors, batteries and transistors.

It did not take long for the electron-device community to start working with this new material for different electronic applications, as it is still a challenge to keep scaling down the device size and ensure that the performance continues to improve. Therefore, scientists are motivated to make devices based on fundamentally different physics by using new 2D material other than a conventional semiconductor. [12] Hence, researchers have been working on synthesize both single-layer and multi-layer graphene with different methods, for example, chemical vapor deposition (CVD) and characterizing the physical and chemical properties of graphene through Raman spectroscopy. [13]

This chapter presents the properties of single layer and multilayer graphene that are grown by CVD method.

3.2 Electrical Properties of Graphene

Graphene is a two-dimensional hexagonal network of carbon atoms with the thickness of one atom.[12] It has several significant physical chemical and electrical properties, for example, mechanical strength, high mobility, unusual Hall Effect and exceptional electronic band gap and high electron mobility. [12,14]

3.2.1 Band Gap

Devices with channels made of large-area graphene cannot be switched off due to the absence of the band gap; however, there are different ways to induce a band gap in graphene by "constraining large-area graphene in one dimension to form graphene nanoribbon", by biasing the bilayer graphene and by applying strain to graphene" [12] (figure 3.1)

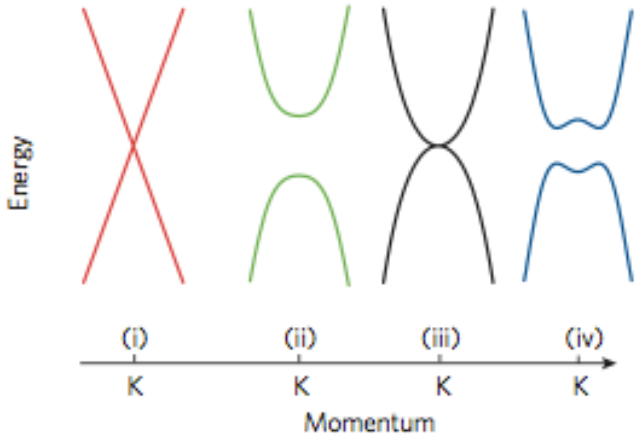

Figure 3-1 Band structure around the K point (i) large-area graphene, (ii) graphene nanoribbons, (iii) unbiased bilayer graphene, (iv) bilayer graphene with an applied perpendicular field. [12]

3.2.2 Electron Mobility

Electron mobility is the most stated feature of graphene; experimental results show that graphene has exceptional high electron mobility at room temperature. For exfoliated graphene on SiO2 substrate, mobilities of 10,000-15,000 $cm^2V^{-1}S^{-1}$ are often measured. Furthermore, without any impurities and ripples, electron mobility could reaches 200,000 $cm^2V^{-1}S^{-1}$, and mobility of 106 $cm^2V^{-1}S^{-1}$ have been reported for suspended graphene.[12] Finally, for large-area graphene grown on nickel and transferred to a substrate (e.g. Si), motilities larger than 3,700 $cm^2V^{-1}S^{-1}$ have been reported. [12]
All these significant mobilities are related to gapless large-area graphene. For graphene nano-ribbons the mobility is lower as they have a band gap. For semiconductor, the mobility decreases as the band gap increases; the same concept has been predicted for graphene nano-ribbons. Therefore, graphene nano-ribbons with a band gap similar to that one in silicon (1.1eV) are expected to have the same mobility of silicon channels in electron devices.[12] Experiments results show that graphene nano-ribbons with 1-10 nm width have electron mobility less than 200 $cm^2V^{-1}S^{-1}$, and 1,500 $cm^2V^{-1}S^{-1}$ for nano-ribbon with a 14 nm width.[12] Although the high mobility of graphene increases the speed of a device, it cannot be used for logic applications since it is difficult to switch off the device. [12]

3.3 Graphene Synthesis

Several methods are used to produce single layer and multilayer graphene. The synthesis procedure can be classified into exfoliation (mechanical or chemical), CVD and reduction of graphene oxide. Exfoliation of graphene is a very popular method that is used in laboratories; however, it is not suitable for producing a wafer-scale graphene in industrial applications. The other two methods both have the potential to be used for industrial purposes.[12,13]

The most promising and cost-effective method for producing high quality graphene over large area is CVD where the graphene layers is grown on a transition metal substrate such as Ni, Pd, Ru, Ir and Cu. In this technique the precursor gases such as CH_4 and H_2 passes through a vacuumed chamber where the substrate is placed at high temperature as high as 1000^oC.[13.15]

Nickel (Ni) is widely used in this process as the substrate because it easily catalyzes the formation of well-oriented graphene. Growing single layer and multilayer graphene through this technique includes two stages: a) decomposition of the carbon source at the metal substrate surface to form single-layer and multilayer graphene, and b) transferring of carbon atoms from metallic substrate to arbitrary substrate.[15,16]

3.4 Raman Spectroscopy

Raman spectroscopy is a powerful technique in characterizing graphene. After the discovery of graphene in 2004, several groups of researchers started to use Raman spectroscopy to gain more understanding of graphene. [13,17]

Raman spectroscopy depends on exciting the material (graphene) by shinning laser on it. Then Raman scattering takes place; this scattering involves intermediate electronic state, resonant Raman scattering using different laser wavelength provides reliable information about the number of graphene layer and characteristics of graphene. [13]

Experimental results show that certain Raman peaks change with the number of graphene layers, leading to Raman fingerprint for single-layer, bilayer and few layer graphene. [17] The most significant graphene Raman shifts are recorded at wavenumbers of 1580 cm^{-1}(G band), , ~2700 cm^{-1} (2D band) and ~1323 cm^{-1} (D band) [16,18] each will be discussed briefly in the following.

3.4.1 The G- Band

The G-band is usually recorded at wavenumber of ~1580 cm^{-1}, and in some cases it can be blue shifted (more than ~1580 cm^{-1}) due to many reasons[13], such as doping, defects, number of layers and strain. [18]

To indicates the number of graphene layers, the G band has to be used with 2D band in order to have an accurate number of layers Figure 3.2 shows Raman spectra of single, bi- and multilayer graphene. As it can be seen from this figure, the G band intensity is increased by decreasing the number of layers, while its bandwidth is decreased. [19]

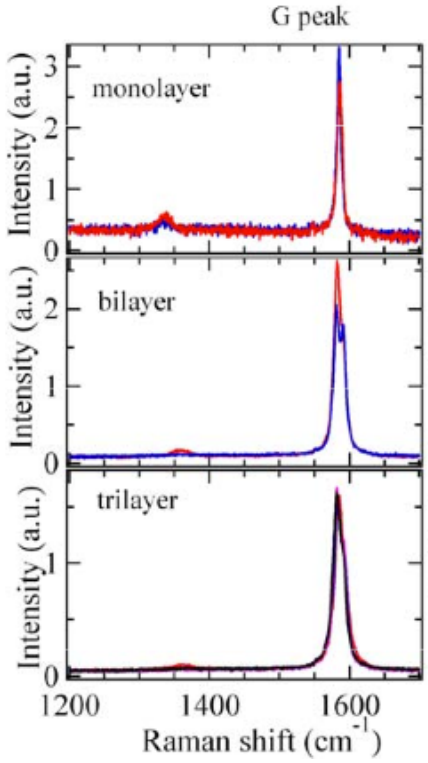

Figure 3-2 G band in Raman spectra of single layer, bilayer and multilayer graphene.[19]

3.4.2 The 2D-Band

The Raman peak at wavenumber of 2680 cm^{-1} is known as 2D band and is the most important feature of Raman spectrum of graphene. Its shape is sensitive to the number of layers, making it a strong indication of the number of graphene layers. Figure 3.3 shows the Raman spectrum of 2D band

in single, bi- and multilayer graphene. From this figure, it can be concluded that the bandwidth of the 2D band increases and its intensity decreases by increasing the number of layers.[18,19]

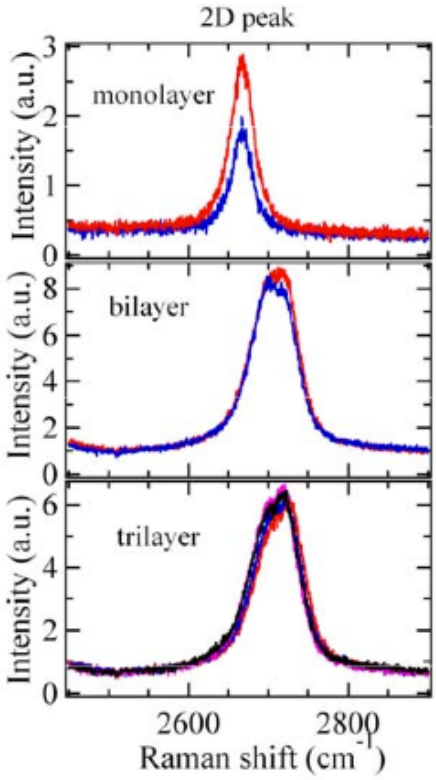

Figure 3-3 2D band in Raman spectrum of single layer, bilayer and multilayerr graphene. [19]

In single layer graphene, the 2D band is sharp and narrow compared to the one in bilayer graphene as clear in figure 3.3. Also, the G band decreases significantly and shifts toward larger wavenumber in single layer graphene, whereas it is more intense in bilayer graphene as can be seen from figure 3.4. [20]

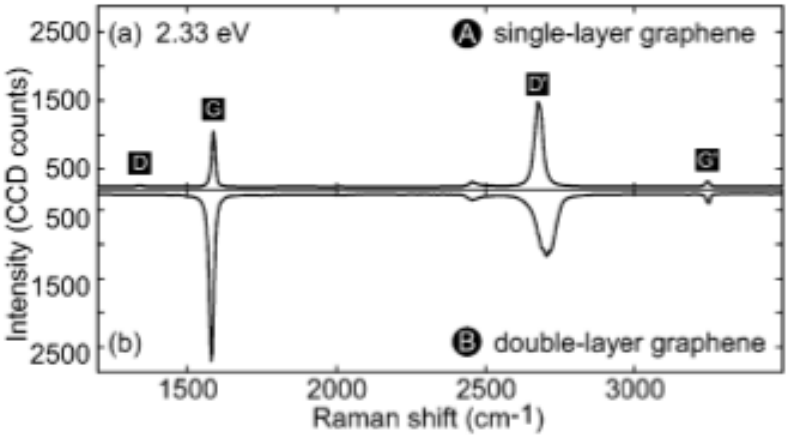

Figure 3-4 The G and 2D bands in single layer and bilayer graphene. [20]. (D' is equivalent to 2D).

3.4.3 The D-Band

The Raman peak at wavenumber of 1323 cm^{-1} is attributed to the D-band, which is an indicator of the presence of defects such as any topographical disorder in the graphene sheet. Figure 3.4 shows a very small D band in single layer graphene, which doesn't appear in bilayer graphene. [20]

3.5 Conclusion

Graphene is the thinnest, lightest and the strongest material ever known, making it a promising candidate material for future revolutionary applications. A growing number of research groups are investigating methods to synthesize and characterize graphene in order to utilize it in various applications. This chapter focused on using graphene in electron applications, and the popular method to achieve high-quality graphene, which is Chemical vapor deposition (CVD). It also showed the major role Raman spectroscopy plays in characterizing graphene films by analyzing the D, G and 2D bands in Raman spectrum.

Chapter 4 Graphene etching and patterning

4.1 Introduction

Producing graphene is the first step toward making graphene-based applications, such as high-speed transistors [21], DNA sequencing and biomechanical sensors. [21] Currently, graphene is being produced by mechanical exfoliating, reduction of graphene oxide and chemical vapor deposition CVD. [21] All these methods are used to produce high quality graphene, however, there are limitations associated with every method. [21]

Making single layer or bilayer graphene is still a challenge due to many technical reasons. The mechanical exfoliating method is time-consuming with low outcome. The technique of graphene oxide reduction and CVD are sensitive to several factors, which are hard to control. Therefore, a new approach towards controlling the number of graphene layers has been introduced. [21]

This chapter presents a method to control the number of graphene layers using Reactive Ion Etching (RIE) using oxygen as etchant environment. The RIE approach was applied on single-layer and multi-layer (three layers) graphene films grown by CVD method. Raman spectra were measured before and after different etching procedures.

The etching process was also used to pattern transfer into a thick, freestanding, reduced graphene-oxide thin film.

4.2 Graphene Etching Using Reactive Ion Etching

The etching process is very useful in controlling the number of graphene layers. It is also important for pattern transfer, as it is the first step in fabricating graphene-based devices.

In this research, the etching process was carried out on multilayer and single layer graphene sheets. The graphene sheets on SiO2/Si substrate were purchased from ACS MATERIALS and Graphene Supermarket Inc. respectively. A simple pattern was used by means of conventional photolithography. The photolithography technique consists of three different steps. In the first step, polystyrene (PS) and positive photoresist (PR) (AZ 300) were coated on the samples surface by means of spin coating technique. The spin-coated samples are baked for a few minutes to dry off the solvent and increase the adhesion between the mask film and the graphene samples. A step pattern was transferred to the graphene sheets samples using UV light at wavelength of 360 nm by means of

appropriate mask as it is shown in Figure 4.1. After an appropriate exposure time which is depended on the resist properties, the UV exposed sample was transferred into a suitable developing solution to remove unexposed (negative resist) or exposed (positive resist) area of photoresist which is called developing process. The last step includes the etching of the transferred pattern by cleaning the etched sample and removing the remaining parts of photoresist by means of MIBK:IPA 3:1 for 10 seconds (figure 4.1).

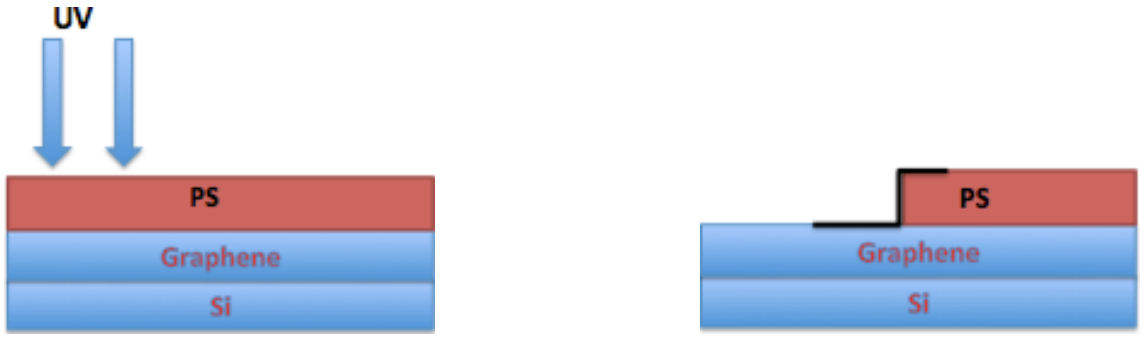

(a) (b)

Figure 4-1 (a) half of the sample was exposed to UV light (b) after the development

In this study, the RIE process was carried out on the transferred pattern in the single layer and the multilayer graphene samples using the following conditions: working pressure of 200 mTorr RF power of 20W (power density 0.01544 W/cm^2), oxygen flow rate of 10 sccm (stander cubic centimeter per minute) and different etching time of 3s, 6s and 9s.
Raman spectroscopy was carried out for all the samples before and after etching.

4.3 Multi-layer Graphene Etching

Multilayer graphene samples with three layers of graphene (1.5nm thickness) were covered with 70nm thick of PS, and different sets of samples were covered with 200nm PR (AZ 300) layer. As shown in figure 1.4, half of the graphene surface was exposed by the oxygen plasma inside the RIE chamber. The etching process can be investigated by Raman spectroscopy of the etchant surface (graphene part) and the number of etched layer can be obtained by calculating the I_{2D} and I_G ratio. Figure 4.3 shows Raman spectrum of a multilayer graphene sample where the PS was used as a protecting mask after different etching times of 3s, 6s and 9s.

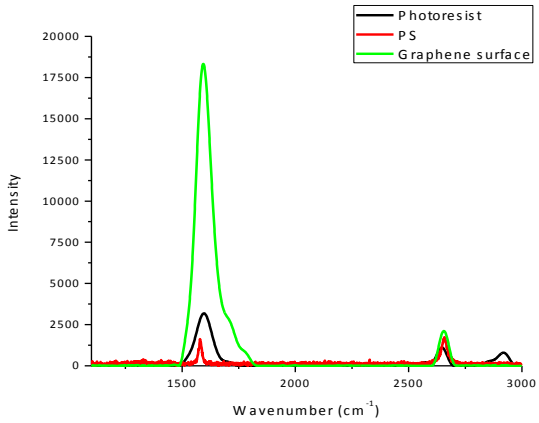

Figure 4-2 Raman spectrum for the samples before etching. PS part, photoresist and graphene part

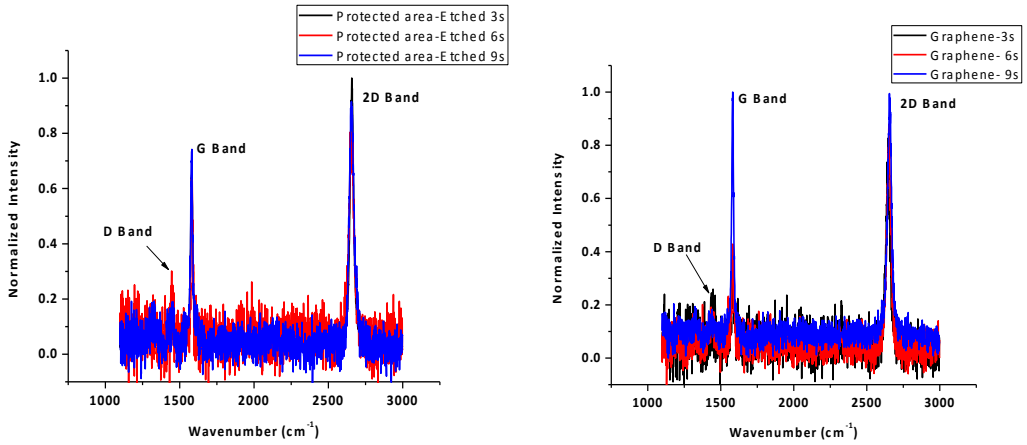

(a) (b)

Figure 4-3 Raman spectrum for the samples after etching (a) Protected part (PS) (b) graphene part.

The Raman spectroscopy provides essential information about graphene properties, such as the number of layers. The intensity ratio between the 2D band and the G band (I2D/IG) is a well-known method of calculating the number of graphene layers. For multilayer graphene sample, the I_{2D}/I_G <1, whereas in the bilayer graphene 1<I2$_D$/I_G <2 and for monolayer graphene the I_{2D}/I_G=2-3. The I_{2D}/I_G ratio of the multilayer graphene sample patterned with PS before and after the etching process is summarized in Table 4.1.

Table 4-1 I_{2D}/I_G ratio of the multilayer graphene sample before and after etching process. The 70nm thick PS film was used as etching mask.

Time (sec)	G-band (cm^{-1})		Intensity		2D-band (cm^{-1})		Intensity		I2D/IG	
	PS	Graphene	PS	Graphene	PS	Graphene	PS	Graphene	PS	Graphene
0	1579.4	1594	1625.5	18329.2	2658.4	2655	1604.4	2109.9	0.98	0.11
3	1582	1581	0.6442	0.5767	2658	2647	1	1	1.55	1.89
6	1582	1581	0.8539	0.8539	2642	2651	1	1	1.17	1.80
9	1580	1582	1	0.8485	2655	2655	0.8842	1	0.99	1.18

Fig.4.3 shows the Raman results of both protected (with PS) and unprotected area for multi-layer graphene after 3s, 6s and 9s of RIE process, and I_{2D}/I_G values for both areas are summarized in Table 4.1. It was found that when using PS as a protecting material after 3s RIE process, the I_{2D}/I_G ratio of unprotected area was increased from 0.11 to 1.89, which indicates that the bi-layer graphene was obtained from 3 layers. By increasing the etching time to 6s the ratio I_{2D}/I_G for graphene was 1.80 which also indicates bi-layer graphene. And 1.18 was achieved when preforming the RIE process for 9s.

Fig.4.3 also shows that the intensity of D band, which is attributed to the production of disorder and defects, [20] increased after preforming the RIE process, whereas it didn't appear in Raman spectrum of the samples before RIE process (fig. 4.2).

Table 4.1 also shows the I_{2D}/I_G for protected areas on the samples before and after RIE process. When preforming 3s etching, the ratio I_{2D}/I_G of the PS part increased from 0.98 to 1.55, which indicates a bi-layer graphene but it was not as high as the graphene part. For 6s etching I_{2D}/I_G was 1.17 and 0.99 after 9s etching.

The same process shown in figure 4.1 was used with 200nm thick positive photoresist PR (AZ 300). Figure 4.2 shows Raman spectrum of PR and graphene part before etching, and figure 4.4 shows Raman spectrum for both PR layer and graphene layer after RIE process for 3s, 6s and 9s.

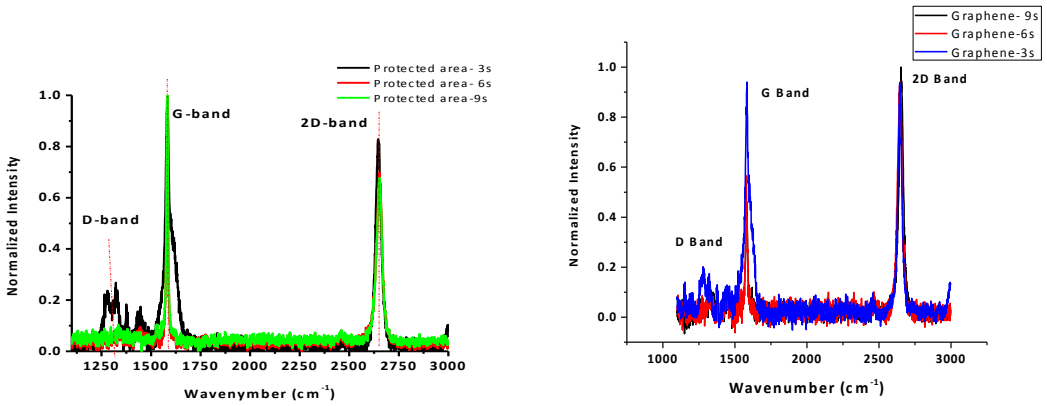

Figure 4-4 Raman spectrum for the samples after etching (a) Protected part (PR) (b) graphene part.

The I_{2D}/I_G ratio of the multilayer graphene sample patterned with PR, before and after etching process is summarized in Table 4.2.

Table 4-2 I_{2D}/I_G ratio of the multilayer graphene sample before and after etching process. The 200nm thick PR film was used as etching mask.

Time (sec)	G-band (cm^{-1})		Intensity		2D-band (cm^{-1})		Intensity		I2D/IG	
	PR	Graphene	PR	Graphene	PR	Graphene	PR	Graphene	PR	Graphene
0	1596.5	1594	3179.5	18329.2	2647.1	2655	1105.6	2109.9	0.34	0.11
3	1581	1582	1	1	2646.2	2643.7	0.6892	0.9897	0.82	0.98
6	1581	1579	1	0.6261	2652.7	2646.2	0.6983	1	0.69	1.57
9	1581	1580	1	0.4150	2652.7	2654.3	0.6578	1	0.67	2.40

Based on the results shown in table 4.2, when using PR as a protecting mask the ratio I_{2D}/I_G for the protected part before and after different etching time was fairly steady. Before etching I_{2D}/I_G was 0.34, which indicates multi-layer graphene, when preforming 3s RIE process I_{2D}/I_G increased slightly to 0.82, which is in the range of multi-layer graphene. With 6s and 9s, RIE process I_{2D}/I_G was 0.69 and 0.67 respectively.

After 3s RIE process, the I_{2D}/I_G ratio of unprotected area was increased from 0.11 to 0.98, which is almost a bi-layer graphene. With a longer etching time (6s) the ratio I_{2D}/I_G for graphene was 1.57, which indicates a bi-layer graphene. Single-layer graphene was obtained when preforming the RIE process for 9s, as I_{2D}/I_G was 2.40.

4.4 Single-layer Graphene Etching

Positive photoresist PR (AZ 300) was used as a mask (200nm) (fig. 4.1) on single-layer graphene grown by CVD. Raman spectrum was obtained before the RIE process (figure 4.5).

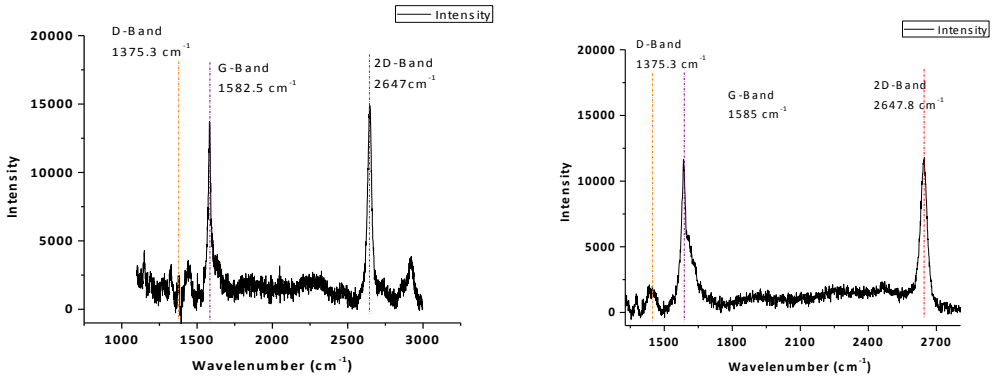

(a) (b)

Figure 4-5 Raman spectrum for single-layer graphene before etching (a) Protected part (PR) (b) graphene part.

After that, the etching was preformed for 3s. Raman spectra for both protected and unprotected parts are shown in figure 4.6; and it is clear that G-band and 2D-band are significantly reduced for the graphene part after 3s RIE process. The ratio I_{2D}/I_G has been calculated for both parts before and after etching as shown in table 4.3.

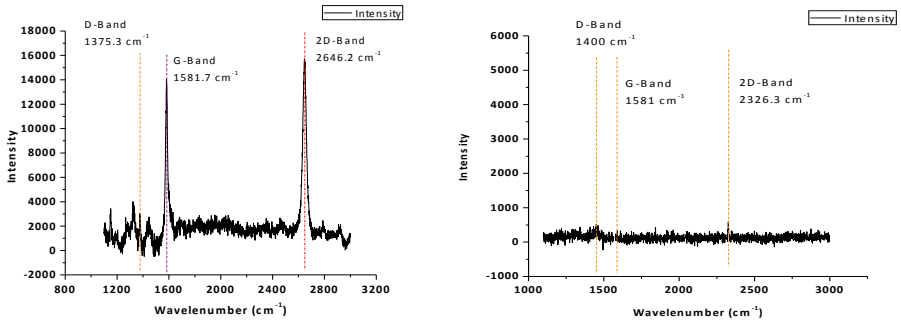

(a) (b)

Figure 4-6 Raman spectrum for single-layer graphene after 3s RIE process (a) Raman spectrum for Photoresist part (b) Raman spectrum for graphene part.

Table 4-3 I_{2D}/I_G ratio of the single-layer graphene sample before and after etching process. The 200nm thick PR film was used as etching mask.

Time (sec)	G-band (cm^{-1})		Intensity		2D-band (cm^{-1})		Intensity		I2D/IG	
	PR	Graphene	PR	Graphene	PR	Graphene	PR	Graphene	PR	Graphene
0	1582.5	1585	13667.7	1155.9	2647	2647.8	14869.5	11650.2	1	1
3	1581.7	1581	13977.1	260.4	2646.2	2326.3	15691.4	531.1	1.1	2.2

According to the data shown in table 4.3, I_{2D}/I_G for protected layer after 3s etching increased slightly from 1 to 1.1. Whereas for the unprotected part the ratio I_{2D}/I_G increased from 1 to 2.2, which indicates a single-layer graphene is etched.

This etching process was preformed on a single-layer graphene patterned with a simple 5µm square using (EBL) and PMMA as a resist. RIE process was preformed for 3s and (SEM) images were taken for the square before and after etching (figure 4.7).

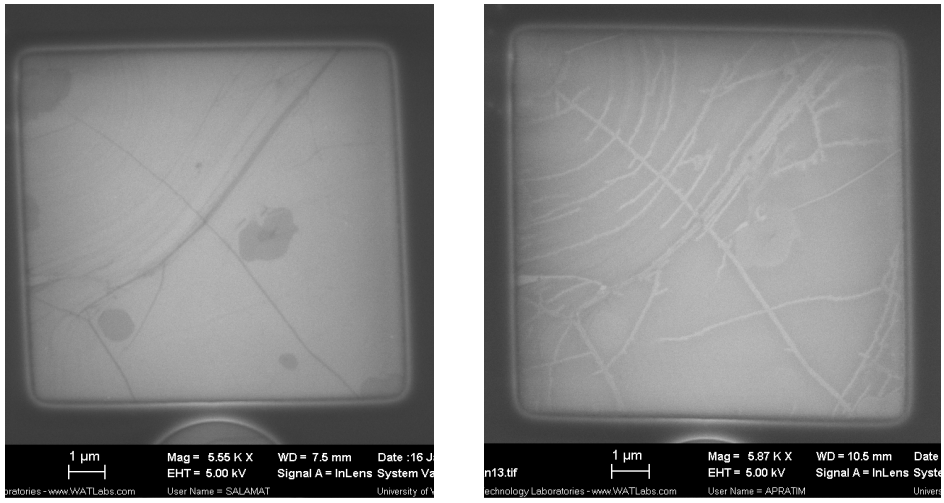

(a) (b)

Figure 4-7 (SEM) images for single-layer graphene after 3s RIE process (a) graphene part before etching (b) graphene part after etching.

As seen in fig.4.7 (a) an island on the graphene part before etching indicating bi-/multi-layer graphene, was faded after the RIE process; also the grain boundaries appeared brighter after 3s etching, which implies that the etching process was successful.

4.5 Patterning Graphene-oxide Film

The etching process has been done on a graphene oxide film that was prepared by filtration of a graphene solution. The solution is a high-concentration graphene (6.2 g/L) exposed to femtosecond laser which has Ti: Sapphire ultrafast regenerative amplifier operating at wavelength of 800 nm, with a repetition rate of 1 kHz, and pulse width of 100 fs and laser energy density of 4.45×10^5 mJ/cm^2 for 60 minutes. Two drops of exposed aqueous graphene oxide solution was filtered using filter membrane with pore-size of 0.05µm. Then the fabricated film on the membrane filter was baked for 6 hours at 50^{o}C in the vacuum oven. The reduced graphene film was achieved by dissolving the

membrane filter in 37% Hydrocholric acid and then transferring it to the silicon wafer followed by 12hr post baking to increase the adhesion between the film and the substrate.

The purpose is to use the etching recipe to transfer a pattern into the graphene oxide film using photolithography. The sample was first covered with AZ 300 photoresist to be used in photolithography process, which implies projecting UV light (1 mW/cm^2 at 360 nm) through a mask with certain pattern (rectangles) to pattern the surface (photoresist). Followed by development process to reveal the pattern (developer MIF319 for 5 seconds). After that, the etching process was preformed using the same RIE process for one minute.

Following that, the photoresist was completely removed with the same developer leaving the final structure on the graphene film (pattern transfer is complete) as shown in figure 4.8. (SEM) images were obtained to show the final pattern (figure 4.9)

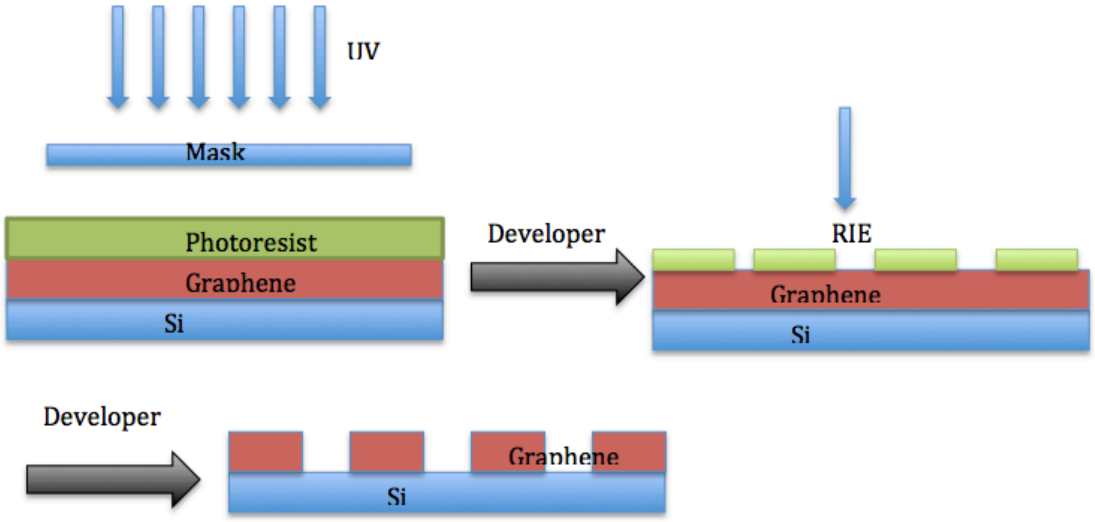

Figure 4-8 Schematic figure of the process of pattering graphene oxide film.

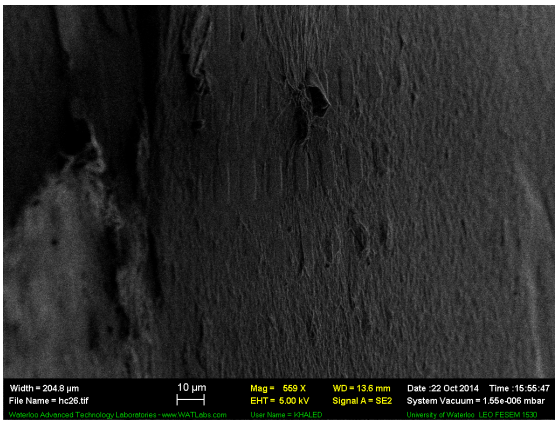

(a)

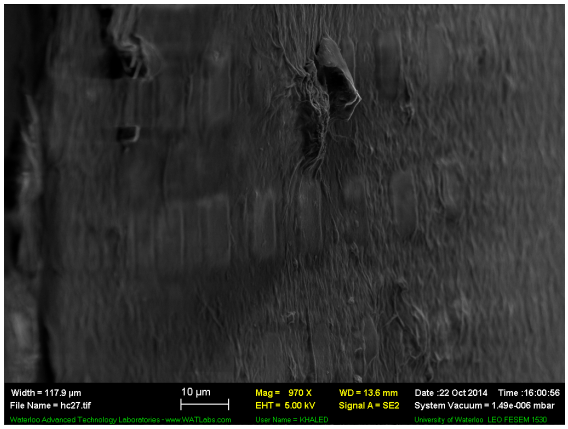

(b)

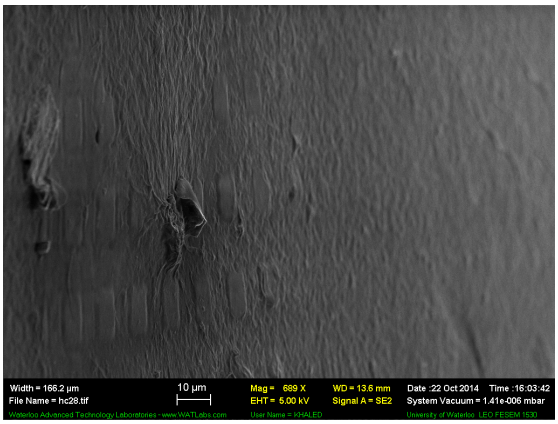

(c)

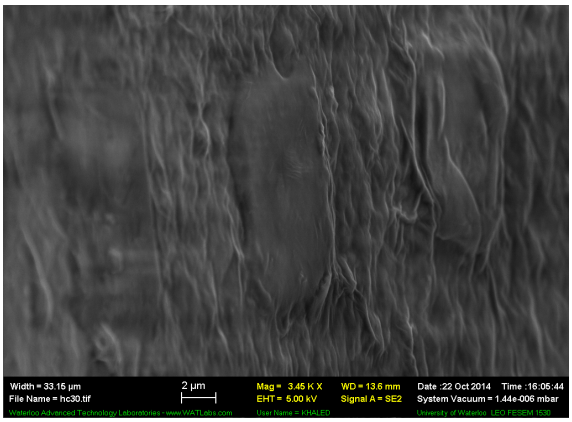

(d)

(e)

(f)

Figure 4-9 SEM images of the graphene oxide sample after etching and pattern transfer process (a), (b) and (c) show the pattern on 10 µm scale (d) show the pattern on 2 µm scale (e) show the pattern

on 2 μm scale with the length dimension of the pattern which is 14 μm (f) show the pattern on 2 μm scale with the width dimension of the pattern which is 4.8 μm

SEM images show that the process of pattern transfer on graphene oxide film using photolithography and RIE etching is successful.

4.6 Conclusion

This chapter presented a method of etching one layer of graphene samples using RIE oxygen plasma. The samples were prepared by chemical vapor deposition CVD, and both multi-layer and single-layer graphene samples were used.

Raman spectrum was collected to characterize the samples before and after the etching process. The number of layers was identified from Raman spectrum by calculating the ratio I2D/IG. The results show that one layer of graphene was etched.

The same etching recipe was used on graphene oxide film along with photolithography process to transfer a pattern to the graphene surface. (SEM) results show the final patterned graphene oxide film.

This etching process provides an effective solution to pattern and etch graphene for different applications.

Appendix A
List of Publications

Journal Paper

[1] W. Alyalak, M. Irannejad, K.H. Hussein, B. Cui, A. Brzezinski, M. Yavuz, "Engineering of bi-/mono- layer grapheme and Graphene oxide free standing film patterning" under preparation for submission

Conferences

[1] M. Irannejad, K. M. Ibrahim, F. Alussail, A. Ramadhan, W. Alyalak,J. Sandeson, Gin Jose, Animesh Jha, Bo Cui, Andrew Brzezinski and Mustafa Yavuz, Leeds, July 2014, Ultrasaft laser interaction with Graphene oxide aqueous solution, International Conference on Optical, Optoelectronic and Photonic Materials and Applications (ICOOPMA 2014).

[2] K. M. Ibrahim, M. Irannejad, A. Ramadhan, W. Alyalak, J. Sandeson, B. Cui, A. Brzezinski, M. Yavuz, Toronto, August 2014, Ultra light interaction with Graphene oxide aqueous solution, IEEE-NANO.

[3] W. Alyalak, M. Yavuz, B. Cui, Lausanne, Switzerland, September 2014, Neutral aurface prepared by vapor coating for PS-b-PMMA self-assembly, 40^{th} international Micro and Nano engineering conference (MNE).

Bibliography

[1] Gu, X., Gunkel, I., & Russell, T. P. (2013). Pattern transfer using block copolymers. *Philosophical Transactions of the Royal Society A: Mathematical, Physical and Engineering Sciences*, *371*(2000), 20120306.

[2] Bucknall, D. (Ed.). (2005). *Nanolithography and patterning techniques in microelectronics*. Elsevier.

[3] Herr, D. J. (2011). Directed block copolymer self-assembly for nanoelectronics fabrication. *Journal of Materials Research*, *26*(02), 122-139.

[4] Bates, F. S., & Fredrickson, G. H. (1990). Block copolymer thermodynamics: theory and experiment. *Annual Review of Physical Chemistry*, *41*(1), 525-557.

[5] Segalman, R. A. (2005). Patterning with block copolymer thin films. *Materials Science and Engineering: R: Reports*, *48*(6), 191-226.

[6] Albert, J. N., & Epps III, T. H. (2010). Self-assembly of block copolymer thin films. *Materials Today*, *13*(6), 24-33.

[7] Chevalier, X., Tiron, R., Upreti, T., Gaugiran, S., Navarro, C., Magnet, S., ... & Hadziioannou, G. (2011, March). Study and optimization of the parameters governing the block copolymer self-assembly: toward a future integration in lithographic proce ss. In *Proc. SPIE* (Vol. 7970, p. 79700Q).

[8] Oria, L., De Luzuriaga, A. R., Chevalier, X., Alduncin, J. A., Mecerreyes, D., Tiron, R., ... & Perez-Murano, F. (2011, March). Guided self-assembly of block-copolymer for CMOS technology: a comparative study between grapho-epitaxy and surface chemical modification. In *SPIE Advanced Lithography* (pp. 79700P-79700P). International Society for Optics and Photonics.

[9] Oria, L., Ruiz de Luzuriaga, A., Alduncin, J. A., & Perez-Murano, F. (2013). Polystyrene as a brush layer for directed self-assembly of block co-polymers. *Microelectronic Engineering*, *110*, 234-240.

[10] Borah, D., Rassapa, S., Shaw, M. T., Hobbs, R. G., Petkov, N., Schmidt, M., ... & Morris, M. A. (2013). Directed self-assembly of PS-b-PMMA block copolymer using HSQ lines for translational alignment. *Journal of Materials Chemistry C*, *1*(6), 1192-1196.

[11] Sohn, B. H., & Yun, S. H. (2002). Perpendicular lamellae induced at the interface of neutral self-assembled monolayers in thin diblock copolymer films. *Polymer*, *43*(8), 2507-2512.

[12] Schwierz, F. (2010). Graphene transistors. *Nature nanotechnology*, *5*(7), 487-496.

[13] Rao, C. N. R., & Sood, A. K. (Eds.). (2013). *Graphene: synthesis, properties, and phenomena*. John Wiley & Sons.

[14] Tsukamoto, T., & Ogino, T. (2011). Control of graphene etching by atomic structures of the supporting substrate surfaces. *The Journal of Physical Chemistry C*, *115*(17), 8580-8585.

[15] Sanyal, B., & Eriksson, O. (Eds.). (2012). *Advanced functional materials: a perspective from theory and experiment* (Vol. 2). Newnes.

[16] Zhang, Y., Zhang, L., & Zhou, C. (2013). Review of chemical vapor deposition of graphene and related applications. *Accounts of chemical research*, *46*(10), 2329-2339.

[17] Wang, H., Wang, Y., Cao, X., Feng, M., & Lan, G. (2009). Vibrational properties of graphene and graphene layers. *Journal of Raman Spectroscopy*, *40*(12), 1791-1796.

[18] Wei, D., Liu, Y., Wang, Y., Zhang, H., Huang, L., & Yu, G. (2009). Synthesis of N-doped graphene by chemical vapor deposition and its electrical properties. *Nano letters*, *9*(5), 1752-1758.

[19] Shukla, A., Kumar, R., Mazher, J., & Balan, A. (2009). Graphene made easy: High quality, large-area samples. *Solid State Communications*, *149*(17), 718-721.

[20] Graf, D., Molitor, F., Ensslin, K., Stampfer, C., Jungen, A., Hierold, C., & Wirtz, L. (2007). Spatially resolved Raman spectroscopy of single-and few-layer graphene. *Nano letters*, *7*(2), 238-242.

[21] Rao, F., Li, W., & Dong, L. (2011, August). Layer engineering of graphene with oxygen plasma etching. In *Nanotechnology (IEEE-NANO), 2011 11th IEEE Conference on* (pp. 1201-1204). IEEE.